R. & M. No. 3813

PROCUREMENT EXECUTIVE, MINISTRY OF DEFENCE

AERONAUTICAL RESEARCH COUNCIL
REPORTS AND MEMORANDA

Cascades with Arbitrary End Wall Contraction

By R. GALAPATTI and W. R. HAWTHORNE
Department of Engineering, University of Cambridge

LONDON: HER MAJESTY'S STATIONERY OFFICE
1978

£4 net

Cascades with Arbitrary End Wall Contraction

By R. GALAPATTI and W. R. HAWTHORNE
Department of Engineering, University of Cambridge

Reports and Memoranda No. 3813*
December, 1976

Summary

A linearised theory for the steady flow of an incompressible, inviscid fluid through a linear cascade of aerofoils set in a channel with contracting or expanding walls is developed first for uniform, potential, flow at inlet and then for a shear flow to represent thick boundary layers near the endwalls. The results are compared with earlier work in which the effects of endwall contraction or expansion are expressed in terms of the Axial Velocity Ratio, i.e. the ratio of downstream and upstream axial velocities at mid-span, and it is shown that these earlier theories are in substantial error because they neglect the effect of the variation of circulation along the aerofoils and the velocities induced by the trailing vortices. Experimental studies of a cascade of NACA 0012 symmetrical uncambered aerofoils at a small deflection and pitch-chord ratio in a porous endwall tunnel, in a tunnel with contracting endwalls, and also with a substantially thickened endwall boundary layer are described and compared with the theory.

* Replaces A.R.C. 37 077

LIST OF CONTENTS

1. Introduction

The flow in two dimensional cascades of aerofoils has been studied extensively both theoretically and experimentally. These studies provide basic data such as lift coefficients, air flow deflections, and losses, which can be used in the design of axial flow turbomachinery. The cascade wind tunnel, which consists of several aerofoils of uniform section spanning a rectangular duct, is the normal tool used for experimental measurements. In such a wind tunnel the flow about the blades or aerofoils is approximately two-dimensional. Exact two-dimensional flow is not generally achieved because the boundary layers on the end walls, that is the walls which contain the span of the aerofoils, generally thickens in the flow through the cascade and therefore produces a contraction of the flow even at the mid-span which can be measured in terms of the change of axial velocity normal to the cascade and is detected by measurements upstream and downstream. In the literature the term Axial Velocity Ratio, that is the ratio of downstream to upstream axial velocity at mid-span is used to define a measure of the contraction effect of these wall boundary layers.

Suction of the boundary through porous end walls has enabled the axial velocity ratio to be controlled, so that data on the variation of cascade deflection and lift coefficient with axial velocity ratio may be obtained. In turbomachinery changes of axial velocity also occur across the rows of compressor or turbine blades, and the effects are often estimated from the data on cascades.

Several attempts have been made to analyse the effects of end wall contraction on cascade performance by using two-dimensional potential flow theories (Pollard and Horlock (1962)[12], Shaalan and Horlock (1968)[15]) where the axial velocity was gradually increased through the cascade, or by using a quasi-two-dimensional theory where the equations are averaged across the contracting passage (Mani and Acosta (1968)[7], Mani, Acosta and Wilson (1974)[8]).

All these theories assume that the contraction of the flow or change of axial velocity is uniform along the span of the aerofoil and therefore there is no change of circulation around the aerofoil in the spanwise direction. In fact an effective contraction of the end walls will not produce a uniform change of axial velocity across the cascade, especially near the end walls. As a consequence the circulation will vary along the span and the flow will become three-dimensional in nature.

This paper presents a small-disturbance theory for the potential flow past a cascade of aerofoils spanning a contracting passage. The theory is fully three-dimensional and takes into account non-uniform lift and shedding of circulation by the blades. Results of calculations and experiments are presented to show that the flow is three-dimensional and that two-dimensional or quasi-two-dimensional theories yield solutions significantly different from the three-dimensional solution.

A small disturbance theory for the shear flow past a cascade with end wall contraction is also presented in order to show the effects of inlet boundary layers on the end walls.

2. Theory

The theoretical approach is based on conventional linearised thin aerofoil theory which is extended to three dimensions and to allow for wall shape and later for inlet shear (see Section 2.7). For a parallel shear flow Honda (1961)[3] reduced the linearised equations of motion, equations (50) to (52) to a partial differential equation for the pressure and defined a potential function whose gradient in the x-direction is proportional to the pressure. When the flow is irrotational there is, in the linearised theory, a similar well-known relationship between the pressure and the potential of the disturbance to the upstream flow, equation (23).

The theory will be developed for the irrotational flow first, but it should be noted that this is only a special case of the flow with shear described in Section 2.7. The flow is assumed to be a perturbation (irrotational) of the uniform upstream flow with velocity U. The fluid is incompressible and inviscid. The perturbation velocities are assumed to be small in comparison with U and are represented by the gradient of a potential. The boundary conditions for the blade surface follow thin aerofoil theory and use the method of solution given by Honda (1961)[3] and others.

2.1. The Disturbance due to the Walls

As the disturbance due to the blades is assumed to be small, the strength of the sheets of sources representing the walls depends only upon the shape of wall, U and the inlet flow angle.

The flow due to the walls is independent of y_1. As the displacement of the streamlines due to walls is small, the boundary conditions at the walls can be satisfied at $z = \pm nl$ rather than at the walls themselves.

Let $\phi_w(x_1, z)$ be the potential of the flow due to the walls. Then,

$$\nabla^2\phi_w = f(x_1) \sum_{n=-\infty}^{+\infty} \delta(z - nl), \tag{1}$$

where $f(x_1)$ is the strength of the sources, and $\delta(z)$ is Dirac's delta function. If the displacement of the streamlines due to the wall is small,

$$f(x_1) = 2a'(x_1)\, U \cos\lambda, \tag{2}$$

where $a'(x)$ is the slope of the wall.

Using the properties of $\delta(z)$, (1) may be written as

$$\nabla^2\phi_w = 2U \cos\lambda\, a'(x_1)\left\{\frac{1}{l} + \frac{2}{l}\sum_{n=1}^{\infty} \cos(2n\pi z/l)\right\} \tag{3}$$

As the flow is symmetrical about $z = \pm nl/2$, ϕ_w may be expanded so that

$$\phi_w = \sum_{n=0}^{\infty} \Phi_{wn}(x_1) \cos(2n\pi z/l) \tag{4}$$

Then, from (3)

$$\frac{d\Phi_{w0}}{dx_1} = 2U \cos\lambda\, a(x_1)/l \quad \text{for} \quad n = 0, \tag{5}$$

and

$$\frac{d^2\Phi_{wn}}{dx_1^2} - \left(\frac{2n\pi}{l}\right)^2 \Phi_{wn} = 4U \cos\lambda\, a'(x_1)/l \quad \text{for} \quad n > 0. \tag{6}$$

Solving for Φ_{wn} by variation of parameters,

$$\begin{aligned}\frac{d\Phi_{wn}}{dx_1} &= 2\frac{U\cos\lambda}{l}\left[\int_{-\infty}^{x_1} a'(t) \exp\{-2n\pi(x_1 - t)/l\}\, dt - \int_{x_1}^{\infty} a'(t) \exp\{-2n\pi(t - x_1)/l\}\, dt\right] \\ &= \frac{2U\cos\lambda}{l} A_n(x_1).\end{aligned} \tag{7}$$

As there is no component of velocity in the y_1 direction,

$$\frac{\partial\phi_w}{\partial y} = -\sin\lambda \sum_{n=0}^{\infty} \frac{d\Phi_{wn}}{dx_1} \cos(2n\pi z/l). \tag{8}$$

2.2. The Disturbance due to the Blades

Let ϕ_t be the potential representing the disturbance due to blade thickness, and ϕ_b the potential of the flow due to blade camber.

If the thickness distribution on each aerofoil is represented by a source distribution q, then, from the assumption of small perturbations.

$$q(x) = 2T'(x)U, \tag{9}$$

where $2T(x)$ is the distribution of thickness. Therefore, q is a function of x only and ϕ_t does not vary in the spanwise direction.

From symmetry,

$$\phi_b(x, y, z) = \sum_{n=0}^{\infty} \Phi_{bn}(x, y) \cos(2n\pi z/l) \tag{10}$$

where the boundary conditions at the walls, $\partial\phi_b/\partial z = 0$ at $z = \pm nl$, are automatically satisfied.

The equation of continuity becomes

$$\nabla_2^2 \Phi_{bn} - (2n\pi z/l)^2 \Phi_{bn} = 0 \tag{11}$$

where

$$\nabla_2^2 = \frac{\partial^2}{\partial x^2} + \frac{\partial^2}{\partial y^2} = \frac{\partial^2}{\partial x_1^2} + \frac{\partial^2}{\partial y_1^2}.$$

The boundary condition at the blade surface is

$$\frac{\partial\phi_b}{\partial y} + \frac{\partial\phi_t}{\partial y} + \frac{\partial\phi_w}{\partial y} = U\left(\frac{d\zeta}{dx} - i\right), \tag{12}$$

where $\zeta(x)$ is the equation of the camberline and i is the angle of incidence with respect to the chord line. Thus, when $n = 0$,

$$\frac{\partial\Phi_{b0}}{\partial y} + \frac{\partial\Phi_{w0}}{\partial y} + \frac{\partial\phi_t}{\partial y} = U\left(\frac{d\zeta}{dx} - i\right) \tag{13}$$

and when $n > 0$,

$$\frac{\partial\Phi_{bn}}{\partial y} + \frac{\partial\Phi_{wn}}{\partial y} = 0 \tag{14}$$

at the blade surface.

It can be shown that

$$\left[\frac{\partial\phi_t}{\partial y}\right]_{y=0} = U\int_{-\frac{1}{2}}^{+\frac{1}{2}} 2T'(\xi)S(x-\xi)\,d\xi, \tag{15}$$

where

$$S(x) = \frac{1}{4s}\left[\frac{\sinh\left\{\frac{2\pi x}{s}\sin\lambda\right\}\cos\lambda - \sin\left\{\frac{2\pi x}{s}\cos\lambda\right\}\sin\lambda}{\cosh^2\left(\frac{\pi x}{s}\cos\lambda\right) - \cos^2\left(\frac{\pi x}{s}\sin\lambda\right)}\right]. \tag{16}$$

Substituting (5) and (15) in (13) the conditions at the blade surface become

$$\frac{\partial\Phi_{b0}}{\partial y} = U\left\{\frac{d\zeta}{dx} + \sin 2\lambda\, a(x\cos\lambda)/l - i - 2\int_{-\frac{1}{2}}^{+\frac{1}{2}} T'(\xi)S(x-\xi)\,d\xi\right\} \tag{17}$$

and

$$\frac{\partial\Phi_{bn}}{\partial y} = U\sin 2\lambda\, A_n(x)/l \quad \text{for} \quad n > 0. \tag{18}$$

Φ_{b0} represents the solution to the two-dimensional flow past a cascade of thin aerofoils. The camber line of the aerofoils has been modified by blade thickness and the contracting end walls. The r.h.s. of equation (17) describes the slope of the modified camber line. The terms $n>0$ represent the component of the flow that is not two-dimensional and they also represent a further distortion of the effective camber line. It should be noted that blade thickness affects only the two-dimensional component of the flow.

As $\int_{-\frac{1}{2}}^{+\frac{1}{2}} q(\xi)\, d\xi = 0$, the effect of ϕ_t is not felt far away from the cascade. The effect of blade thickness is neglected in some of the subsequent equations.

2.3. Quasi-Two-Dimensional Flow

If the equation of continuity is averaged across the passage,

$$\nabla_2^2 \bar{\Phi} + \frac{1}{2h}\left[\frac{\partial \phi}{\partial z}\right]_a^{l-a} = 0 \tag{19}$$

where $h(x_1) = \frac{1}{2}l - a(x_1)$, $\bar{\Phi} = 1/2h \int_a^{l-a} \phi\, dz$ and $\phi = \phi_w + \phi_b + \phi_t$. The r.h.s. of equation (19) is zero because the equation is not integrated across the sources at $z = 0$ and l. As $\partial\phi/\partial z = \pm U \cos\lambda\, a'(x_1)$ near the walls,

$$\nabla_2^2 \bar{\Phi} + \frac{h'(x_1)}{h(x_1)} U \cos\lambda = 0. \tag{20}$$

Equation (20) represents exactly the model used by Pollard and Horlock (1962) in which the increase in axial velocity was brought about by placing strip sources in the blade passage. The modified equation of continuity obtained by Shaalan and Horlock (1968)[12],

$$\nabla_2^2 \phi = -\frac{1}{x_1}\frac{\partial \phi}{\partial x_1} \tag{21}$$

and the passage averaged equation given by Mani and Acosta (1968)[7]

$$\nabla_2^2 \phi + \frac{h'}{h}\frac{\partial \phi}{\partial x_1} = 0, \tag{22}$$

reduce to equation (20) when all second order terms are properly neglected.

2.4. Downstream Flow

In a small perturbation flow,

$$\begin{aligned} p - p_{-\infty} &= -\rho U \frac{\partial \phi}{\partial x} \\ &= -\rho U\left[\cos\lambda \frac{\partial \phi_w}{\partial x_1} + \frac{\partial \phi_b}{\partial x}\right]. \end{aligned} \tag{23}$$

Far downstream, where the walls are parallel, the pressure becomes uniform so that all terms except those for $n = 0$ disappear, giving the pressure rise coefficient,

$$C_p = \frac{p_\infty - p_{-\infty}}{\frac{1}{2}\rho U^2} = C_{p_{b0}} - \frac{4a(\infty)}{l}\cos^2\lambda, \tag{24}$$

where $C_{p_{b0}}$ is the pressure rise coefficient for a two-dimensional flow through a cascade whose camber line is given by (17).

Let the deflection of the flow be given by

$$\beta = \beta_0 + \sum_{n=1}^{\infty} \beta_n \cos(2n\pi z/l), \tag{25}$$

where

$$\beta_n = \frac{1}{U}\frac{\partial \Phi_{bn}}{\partial y} + \frac{1}{U}\frac{\partial \Phi_{wn}}{\partial y}$$
$$= \beta_{bn} + \beta_{wn}, \tag{26}$$

where the derivatives are evaluated at $x = +\infty$.

From (5) $\beta_{w0} = a(\infty)\sin 2\lambda/l$ and because by inspection of (7)

$$\frac{d\Phi_{wn}}{dx_1} \to 0 \quad \text{as} \quad x_1 \to \infty,$$

β_{wn} for $n > 0$ also vanishes for $x = \infty$.

2.5. Solution

Solutions to the problem posed by (11) and (18) have been given by Honda (1961)[3], Nally and Hawthorne (1968)[10] and Namba (1969)[11]. The solution assumed is

$$\phi_{bn}(x, y) = -\int_{-\frac{1}{2}}^{+\frac{1}{2}} M_n(\xi) \sum_{m=-\infty}^{+\infty} \int_{-\infty}^{x} \frac{\partial}{\partial y}\left[K_0\left(\frac{2n\pi}{l} R_m\right)\right] dx\, d\xi, \tag{27}$$

where K_0 is the modified Bessel function of the second kind of order zero and

$$R_m = \{(x - \xi - ms\sin\lambda)^2 + (y - ms\cos\lambda)^2\}^{\frac{1}{2}}. \tag{28}$$

When $n = 0$, the solution to equations (11) and (17), neglecting the effect of blade thickness, is

$$\Phi_{b0}(x, y) = -\int_{-\frac{1}{2}}^{+\frac{1}{2}} M_0(\xi) \sum_{m=-\infty}^{+\infty} \int_{-\infty}^{x} \frac{\partial}{\partial y}(\log R_m)\, dx\, d\xi, \tag{29}$$

where $2\pi M_0(x)$ is the distribution of bound vorticity on each blade. Nally and Hawthorne (1968)[10] show that the solution given by (27) also corresponds to a distribution of bound vorticity of strength $2\pi M_n(x)$ on each blade. The bound vorticity on each blade may now be expressed as

$$\gamma(x, z) = 2\pi \sum_{n=0}^{\infty} M_n(x)\cos(2n\pi z/l). \tag{30}$$

From (27) and (29)

$$\lim_{x \to -\infty} \frac{\partial \phi_{bn}}{\partial y} = 0 \quad \text{for all} \quad n \tag{31}$$

and

$$\lim_{x \to -\infty} \frac{\partial \Phi_{wn}}{\partial y} = 0 \quad \text{for all} \quad n \tag{32}$$

as $a(x) = 0$ at $x = -\infty$.

Honda (1961)[3] shows that at downstream infinity

$$\frac{\partial \Phi_{b0}}{\partial y} = -\frac{2\pi}{s}\cos\lambda \int_{-\frac{1}{2}}^{+\frac{1}{2}} M_0(\xi)\, d\xi \quad \text{for} \quad n = 0, \tag{33}$$

and

$$\frac{\partial \phi_{bn}}{\partial y} = -\frac{2n\pi^2}{l}\frac{\cosh\{(n\pi/l)(s\cos\lambda - 2y)\}}{\sinh[(n\pi/l)s\cos\lambda]} \int_{-\frac{1}{2}}^{+\frac{1}{2}} M_n(\xi)\, d\xi, \tag{34}$$

where $0 < y < s \cos \lambda$ and $n > 0$. Averaging equation (34) between $y = 0$ and $s \cos \lambda$, we have

$$\frac{\partial \Phi_{bn}}{\partial y} = \frac{2\pi}{s \cos \lambda} \int_{-\frac{1}{2}}^{+\frac{1}{2}} M_n(\xi)\, d\xi \quad \text{for} \quad n > 0. \tag{35}$$

The local lift coefficient at a spanwise station may be obtained from equation (30)

$$C_L(z) = \frac{4\pi}{U} \sum_{n=0}^{\infty} \left[\int_{-\frac{1}{2}}^{+\frac{1}{2}} M_n(\xi)\, d\xi \right] \cos(2n\pi z/l). \tag{36}$$

From (25), (33) and (35) we have

$$\beta_0 = \frac{a_\infty}{l} \sin 2\lambda + \frac{2\pi \cos \lambda}{Us} \int_{-\frac{1}{2}}^{+\frac{1}{2}} M_0(\xi)\, d\xi, \tag{37}$$

and

$$\beta_n = \frac{2\pi}{Us \cos \lambda} \int_{-\frac{1}{2}}^{+\frac{1}{2}} M_n(\xi)\, d\xi, \tag{38}$$

It can also be shown that

$$C_p = \frac{4\pi \sin \lambda}{Us} \int_{-\frac{1}{2}}^{+\frac{1}{2}} M_0(\xi)\, d\xi - 4 \frac{a_\infty}{l} \cos^2 \lambda. \tag{39}$$

$M_n(x)$ can be obtained by solving an integral equation of the type

$$f(x) = -\int_{-\frac{1}{2}}^{+\frac{1}{2}} M_n(\xi) \sum_{m=-\infty}^{+\infty} \int_{-\infty}^{x} \frac{\partial^2}{\partial y^2} \left[K_0\left(\frac{2n\pi}{l} R_m \right) \right] dx\, d\xi \quad \text{at} \quad y = 0, \tag{40}$$

$$= \int_{-\frac{1}{2}}^{+\frac{1}{2}} h_n(x - \xi) M_n(\xi)\, d\xi, \tag{41}$$

where $f(x)$ represents the right hand side of equation (18). The complete solution to equation (41) must also include the singular solution such that

$$\int_{-\frac{1}{2}}^{+\frac{1}{2}} h_n(x - \xi) N_n(\xi)\, d\xi = 0. \tag{42}$$

Then

$$M_n(x) = M_n'(x) + k_n N_n(x), \tag{43}$$

where M_n' is a solution to equation (41) and k_n is a constant. The constant k_n is determined by the trailing edge condition, i.e. by putting $M_n(\frac{1}{2}) = 0$, so that

$$k_n = -M_n'(\tfrac{1}{2}) / N_n(\tfrac{1}{2}). \tag{44}$$

2.6. The Closely Spaced Cascade

In a cascade with closely spaced blades in two-dimensional flow the outlet angle becomes nearly equal to the blade exit angle. Therefore from equation (17)

$$\beta_0 - \beta_{2D} = \sin 2\lambda\, (a_\infty - a_{t.e.})/l. \tag{45}$$

The subscript '2*D*' refers to two-dimensional flow without endwall contraction and '*t.e.*' refers to the trailing edge. Equation (39) shows that the terms $n>0$ do not contribute to the pressure rise through the cascade. Hence from equation (23)

$$\frac{\partial \phi}{\partial x}=0 \quad \text{when} \quad n>0,$$

because the pressure is uniform far downstream. On the other hand these terms contribute to the y component of velocity $\partial\phi_{bn}/\partial y = -\gamma_n/s \cos\lambda$, which can be resolved into components $-\gamma_n/s$ and $\gamma_n \tan\lambda/s$ in the pitchwise (y_1) and axial (x_1) directions respectively.

Many bladed cascades are often treated as actuator discs across which there is a change in flow angle, pitchwise velocity and pressure (see Horlock (1958)[4] for an exposition of the theory). The actuator disc theory for an isolated blade row shows that half the change in axial velocity through the cascade occurs at the disc. Therefore, if we make the simple assumption that the disc is at the trailing edge,

$$-\tfrac{1}{2}\gamma_n \tan\lambda \sin\lambda/s - \gamma_n \cos\lambda/s = \frac{U \sin 2\lambda}{l} A_{n_{t.e.}},$$

i.e.

$$\gamma_n = -2\frac{U \sin 2\lambda}{l} \cdot \frac{s \cos\lambda}{1+\cos^2\lambda} A_{n_{t.e.}}, \tag{46}$$

where γ_n would correspond to $2\pi \int_{-\frac{1}{2}}^{+\frac{1}{2}} M_n(\xi)\, d\xi$ in (38). Therefore,

$$\beta_n = \gamma_n / Us \cos\lambda$$

$$= \frac{-2 \sin 2\lambda}{l(1+\cos^2\lambda)} A_{n_{t.e.}}. \tag{47}$$

The total deflection due to a cascade of closely spaced blades is therefore approximately

$$\beta = \beta_{2D} + \sin 2\lambda\ (a_\infty - a_{t.e.})/l - \frac{2 \sin 2\lambda}{1+\cos^2\lambda} \cdot \frac{1}{l} \sum_{n=1}^{\infty} A_{n_{t.e.}} \cos(2n\pi z/l). \tag{48}$$

The effects of endwall contraction have been expressed in the literature in terms of the change in deviation angle, δ, that is the angle between the tangent to the camber line at the trailing edge and the far downstream flow angle (*see* Fig. 8). Attempts have been made in the literature to correlate the effect of axial velocity ratio (AVR) at mid-span on deviation by using $[\delta - \delta_{2D}]/[\theta(\text{AVR}-1)]$ as a parameter, where δ_{2D} is the value of δ for no contraction, i.e. AVR = 1, and θ is the camber of the aerofoil. Our equation (48) may be used to derive a mid-span deviation rule in the form

$$\frac{\delta - \delta_{2D}}{\text{AVR}-1} = \frac{B}{\text{AVR}},$$

where

$$B = \frac{\sin\lambda}{1+\cos^2\lambda} \cdot \frac{l}{\pi} \left\{ \log\left(\frac{2}{1+e^{-2\pi \cos\lambda/l}} \right) \right\}. \tag{49a}$$

When the aspect ratio (l) is small

$$B = \frac{\sin\lambda}{1+\cos^2\lambda} \cdot \frac{l}{\pi} \log 2, \tag{49b}$$

and when l is large

$$B = \frac{\sin\lambda \cos\lambda}{1+\cos^2\lambda}. \tag{49c}$$

It has been assumed that $a'(x_1)$ is a constant in the blade passage and zero everywhere else when deriving equations (49).

It should be emphasised that these results are based on the simplest of assumptions. More accurate results would be obtained by a through flow analysis.

The results given in equations (49) may be compared with the approximations given by Lakshiminarayana (1970 p. 127)[6] which have the same form, but different values for B. The equation (49a) is used in the preparation of the mid-span curves in Fig. 5.

2.7. The Effect of Inlet Shear

If the flow is assumed to be a small disturbance of a parallel shear flow $U(z)$, the equations of motion are, when second order quantities are neglected,

$$U\frac{\partial u}{\partial x} + w\frac{dU}{dz} + \frac{1}{\rho}\frac{\partial p}{\partial x} = 0, \tag{50}$$

$$U\frac{\partial v}{\partial x} + \frac{1}{\rho}\frac{\partial p}{\partial y} = 0, \tag{51}$$

and

$$U\frac{\partial w}{\partial x} + \frac{1}{\rho}\frac{\partial p}{\partial z} = 0, \tag{52}$$

where u, v and w are the components of the disturbance velocity.

The equation of continuity is

$$\frac{\partial u}{\partial x} + \frac{\partial v}{\partial y} + \frac{\partial w}{\partial z} = 0. \tag{53}$$

Honda (1961)[3] has shown that a potential function,

$$\phi = -\int_{-\infty}^{x} p/\rho \, dx, \tag{54}$$

would satisfy the equations of motion if

$$u = \frac{1}{U}\frac{\partial \phi}{\partial x} - \frac{U'}{U^2}\int_{-\infty}^{x} w \, dx, \tag{55}$$

$$v - v_{-\infty} = \frac{1}{U}\frac{\partial \phi}{\partial y}, \tag{56}$$

and

$$w = \frac{1}{U}\frac{\partial \phi}{\partial z}. \tag{57}$$

The equation of continuity may now be written as

$$\frac{\partial^2 \phi}{\partial x^2} + \frac{\partial^2 \phi}{\partial y^2} + U^2\left[\frac{\partial}{\partial z}\left(\frac{1}{U^2}\frac{\partial \phi}{\partial z}\right)\right] = 0. \tag{58}$$

p would also satisfy equation (58). Honda[3] also showed that if

$$\phi = \sum_k F(k)Z(z, k)\Phi(x, y, k), \tag{59}$$

then

$$\frac{d}{dz}\left(\frac{1}{U^2}\frac{dZ}{dz}\right) + k^2\frac{Z}{U^2} = 0, \tag{60}$$

and

$$\nabla_2^2\Phi - k^2\Phi = 0. \tag{61}$$

If the boundary condition $w = 0$ at $z = 0$ and l is applied, the solution to (60) yields a complete set of orthogonal eigenfunctions $= [Z(z, k)]/U$ such that

$$\int_0^l \frac{Z(z, i)Z(z, j)}{U^2}dz = 0 \quad \text{when} \quad i \neq j. \tag{62}$$

$Z(z, k)$ is normalised so that

$$\frac{1}{l}\int_0^l \frac{Z^2(z, k)}{U^2}dz = 1. \tag{63}$$

Let the disturbance to the flow be represented by

$$\phi = \phi_b + \phi_w, \tag{64}$$

where ϕ_b is the disturbance due to the blades and ϕ_w the disturbance due to the walls. As both ϕ_w and ϕ_b represent small disturbances to the mainstream flow, $U(z)$, let us assume that ϕ_b and ϕ_w each satisfy equation (59). The coordinate axes remain as shown in Figure 1.

(a) The Disturbance Due to the Walls

Let the contracting walls be represented by sheets of sources at $z = 0, \pm l, \pm 2l \ldots$. The strength of these sources are given by

$$f(x_1) = 2a'(x_1)U_1 \cos\lambda, \tag{65}$$

where U_1 is the value of $U(z)$ near the wall.

The equation of continuity is

$$\nabla_2^2\phi_w + U^2\frac{\partial}{\partial z}\left(\frac{1}{U^2}\frac{\partial\phi_w}{\partial z}\right) = 2a'(x_1)U_1\cos\lambda \sum_{n=-\infty}^{+\infty}\delta(z - nl). \tag{66}$$

Let $\phi_w = \sum_k F_w(k)Z(z, k)\Phi_w(x, y, k)$.

The boundary conditions at the walls may be satisfied by writing $dZ/dz = 0$ at $z = 0$ and l. If we also assume that $Z(z, k)$ is the complete set of orthogonal functions described by (62) and (63), the series of delta functions may be expressed as

$$\sum_{n=-\infty}^{\infty}\delta(z - nl) = \sum_k G(k)Z(z, k). \tag{67}$$

Then from (65) and (66) we have

$$\frac{d}{dz}\left(\frac{1}{U^2}\frac{dZ}{dz}\right) + k^2\frac{Z}{U^2} = 0, \tag{60}$$

and

$$\nabla_2^2\Phi_w - k^2\Phi_w = 2a'(x_1)U_1\cos\lambda\, G(k)/F_w(k). \tag{68}$$

Φ_w is a function of x_1 only. Therefore

$$\frac{d\Phi_w}{dx_1} = \frac{G(0)}{F_w(0)}\cdot 2U_1\cos\lambda\, a(x_1) \quad \text{for} \quad k=0 \tag{69}$$

$$= \frac{G(k)}{F_w(k)}U_1\cos\lambda\, A_k(x_1) \quad \text{for} \quad k>0, \tag{70}$$

where

$$A_k(x_1) = \int_{-\infty}^{x_1} a'(t)\exp\{-k(x_1-t)\}\,dt - \int_{x_1}^{\infty} a'(t)\exp\{-k(t-x_1)\}\,dt. \tag{71}$$

As $\partial\Phi_w/\partial y_1 = 0$,

$$\frac{\partial\Phi_w}{\partial y} = -\sin\lambda\frac{d\Phi_w}{dx_1}. \tag{72}$$

It should also be noted that

$$\lim_{x_1\to\infty} A_k(x_1) = 0 \quad \text{for} \quad k>0. \tag{73}$$

(b) The Disturbance Due to the Blades

The equations governing ϕ_b follow Honda[3].

If

$$\phi_b = \sum_k F(k)Z(z,k)\Phi_b(x,y,k), \tag{74}$$

then

$$\frac{d}{dz}\left(\frac{1}{U^2}\frac{dZ}{dz}\right) + k^2\frac{Z}{U} = 0, \tag{60}$$

and

$$\nabla_2^2\Phi_b - k^2\Phi_b = 0. \tag{75}$$

The boundary condition at the walls yield the same set of orthogonal functions $Z(z,k)$ as before. The boundary condition at the blade surface becomes

$$\frac{1}{U^2}\sum_k F(k)Z(z,k)\left[\frac{\partial\Phi_b}{\partial y}(x,0,k) + \frac{F_w(k)}{F(k)}\frac{\partial\Phi_w}{\partial y}(x,0,k)\right] = \frac{d\zeta}{dx} - i. \tag{76}$$

Therefore,

$$\frac{1}{U^2}\sum F(k)Z(z,k) = 1, \tag{77}$$

and

$$\left[\frac{\partial \Phi_b}{\partial y}\right]_{y=0} = \frac{d\zeta}{dx} - i + \frac{G(0)}{F(0)} U_1 \sin 2\lambda \, a(x \cos \lambda) \quad \text{for} \quad k = 0, \tag{78}$$

$$= \frac{d\zeta}{dx} - i + \frac{1}{2} \frac{G(k)}{F(k)} U_1 \sin 2\lambda \, A_k(x \cos \lambda) \quad \text{for} \quad k > 0. \tag{79}$$

Therefore the problem reduces to that described by Honda (1961)[3] with different boundary conditions at the blades.

It can be shown that

$$F(0) = Z(z, 0) = \left[\frac{1}{l} \int_0^l \frac{dz}{U^2}\right]^{\frac{1}{2}} \text{ for } \quad k = 0, \tag{80}$$

$$F(k) = \frac{1}{l} \int_0^l Z(z, k) \, dz \text{ for } \quad k > 0, \tag{81}$$

and

$$G(k) = \frac{1}{l} \frac{Z(0, k)}{U_1^2}. \tag{82}$$

The solution to (75) is given by Honda as

$$\Phi_b(x, y, k) = \int_{-\frac{1}{2}}^{+\frac{1}{2}} \left[\sum_{m=-\infty}^{+\infty} \int_{-\infty}^{x} \frac{\partial}{\partial y} K_0(kR_m) \, dx\right] M_k(\xi) \, d\xi. \tag{83}$$

The expression for R_m is given by (28). It is possible to derive expressions for lift, pressure rise and flow deflection from the results obtained by Honda (1961)[3] and Nally and Hawthorne (1969)[10].

The local lift at a spanwise station is

$$L(z) = 2\pi\rho \sum_k F(k) Z(z, k) \int_{-\frac{1}{2}}^{+\frac{1}{2}} M_k(\xi) \, d\xi, \tag{84}$$

$$p_\infty - p_{-\infty} = \left[\rho 2F^2(0) \frac{\pi}{s} \sin \lambda \int_{-\frac{1}{2}}^{+\frac{1}{2}} M_0(\xi) \, d\xi - 2G(0)F(0)U_1 \cos^2 \lambda \, a(\infty)\right], \tag{85}$$

$$\frac{\bar{v}_\infty}{U} - \frac{\bar{v}_{-\infty}}{U} = -\frac{1}{U^2}\left\{F(0)Z(z, 0)\frac{2\pi}{s} \cos \lambda \int_{-\frac{1}{2}}^{+\frac{1}{2}} M_0(\xi) \, d\xi + \sum_{k>0} F(k)Z(z, k)\frac{2\pi}{s \cos \lambda} \int_{-\frac{1}{2}}^{+\frac{1}{2}} M_n(\xi) \, d\xi \right.$$

$$\left. + G(0)Z(z, 0)U_1 \sin 2\lambda \, a(\infty)\right\}, \tag{86}$$

where

$$\bar{v} = \frac{1}{s \cos \lambda} \int_0^{s \cos \lambda} v \, dy.$$

Kotansky (1965)[5] has shown that relatively simple eigenfunctions $Z(z, k)$ can be obtained if the velocity profile $U(z)$ consists of a combination of straight lines. The numerical solution was obtained along these lines using a procedure developed by Nally and Hawthorne[10].

3. Numerical Results and Discussion

In this section we describe a number of results obtained using the preceding theory. The inlet flow velocity except where otherwise stated is uniform and parallel.

The variation in lift caused by end wall contraction depends on the local increase in axial velocity $\partial\phi_w/dx_1$. Figures 2 and 3 show the considerable spanwise variations in $\partial\phi_w/dx_1$ that are caused by a linear contraction of the end walls. They show that if a cascade with uniform inlet velocity is placed within such a contracting passage there will be considerable variation of lift and outlet angle along the span.

The actuator disc solution, that is the solution for $s = 0$ which corresponds to an infinite number of closely spaced blades, is compared with the exact solution for increasing values of pitch-chord ratio for a flat plate compressor cascade in Fig. 4. Unless otherwise stated, a linear contraction of the end walls that begins at the leading edge and ends at the trailing is assumed in every calculation. The end wall contraction causes flow deflection to decrease near the wall and increase at mid-span. The spanwise variations decrease with the increase in pitch-chord ratio. Fig. 5 shows the influence of stagger angle on the changes in deviation angle at mid-span and near the wall. These calculations were made using the actuator disc theory for two aspect ratios. The curves show that end wall effects reach a peak when inlet flow angle is between 50 and 70 degrees. Two points in the figure show the solutions for a flat plate cascade with $s = 1{\cdot}5$ (note the chord = 1).

The effects of aspect ratio and wall shape on deviation angle are shown in Fig. 6. The solution for $n = 0$, which coincides with the two-dimensional solution given by Pollard and Horlock (1962)[12] expressed in equation (20), is also given, and it underestimates the increase in mid-span turning angle by about 50 per cent. The main reason for this discrepancy is that the $n = 0$ term does not contain the effect of the spanwise variation of axial velocity in the passage and the effects of the circulation shed from the blades. These are contained in the terms $n > 0$ and may be seen to have an effect at all points along the span. An improvement of the use of equation (20) might be obtained by applying it to several stream sheet thicknesses across the passage.

In Fig. 6 are also shown the results obtained for a parabolic wall shape. The shape of wall used in the calculation is given by $a(x_1) = a_\infty(\frac{1}{2}+x_1)(3/2-x_1)$.

If the local axial velocity causes an apparent change in the camber line as shown by equations (17) and (18), then from Figs. 2 and 3 it is clear that the relative positions of the cascade and the contraction will also have an influence on the outlet angles. This effect is shown in Fig. 7 where the position of a linear end wall contraction equal in length to the axial chord length was changed relative to the blades.

The calculations presented so far have made it clear that the position and shape of the end wall contraction has a very significant influence on the outlet flow angle. In other words it appears that it is not possible by simply measuring inlet and outlet velocities at mid-span in a cascade experiment to ensure that the effects of flow contraction are properly determined. This conclusion may be explained physically by noting that the circulation around the blades depends on the details of the flow. The fact that the solution is a function of the shape and position of the end wall contraction throws some doubt on the usefulness of current experimental cascade data, in which the effective wall shape is not known, in determining the so-called axial velocity ratio effects across a cascade.

A calculation to show the effect of a parallel shear flow at inlet was done for comparison with test results to be described below (Fig. 13).

4. The Experimental Program

The experimental program was carried out in the low speed cascade wind tunnel at the S.R.C. Turbomachinery Laboratory, Cambridge. The tunnel was fitted with a variable incidence mechanism and side wall suction. A seven bladed cascade of uncambered aerofoils of the shape NACA 0012 was tested. The details of the cascade are given below:

Stagger angle = 45°
Camber angle = 0
Max. thickness = 0·12 chord at 30% chord
Chord = 12 inches
Aspect ratio = 2
Pitch/chord = 0·64
Axial chord = 8·48 inches

The porous side walls projected 5 inches upstream and downstream of the cascade in the axial direction. The term 'unrestricted suction' will refer to tests where side wall suction was applied through the total area of porous wall, 'restricted suction' refers to tests where side wall suction was applied only within the blade row. Static pressure tappings were located on the central blade at five spanwise positions, and the outlet flow was traversed in a plane one axial chord length downstream of the trailing edge plane. The values presented have been made non-dimensional with respect to the measured mid-span velocity upstream.

More details of apparatus and instrumentation are given by Galappatti (1973)[2]. Test were also carried out after fitting contracting solid end walls to the cascade. The shape of the contraction is shown in Fig. 8. All tests were carried out at a Reynolds number of $3{\cdot}70 \times 10^5$. The details of the tests are given in Table 1.

TABLE 1

Test	Inlet flow	Side walls	Side wall suction	Inlet flow angle	Extent of suction	AVR
A/0	uniform	porous	1, 2, 3 & 4	49°	unrestricted	<1
A/1	uniform	porous	none	49°	—	1·049
A/2	uniform	porous	5	49°	unrestricted	0·947
A/3	uniform	porous	6	49°	restricted	0·966
A/4	uniform	porous	6	51°	restricted	0°982
A/5	uniform	porous	7	49°	restricted	0·943
B/1	uniform	built-up	none	49°	—	1·251
B/2	shear	built-up	none	49°	—	1·154

5. Discussion

It was possible to determine the two-dimensional performance of the cascade by plotting the variation of mid-span outlet angle with AVR, as shown in Fig. 9. The variation of lift coefficient is also shown. The outlet angle for an axial velocity ratio of unity was found to be 47·7 degrees which represents a deviation angle of 2·7 degrees at an incidence of 4 degrees. Potential flow theory predicts a negligible deviation angle for the flow past a flat plate cascade of the same geometry with the same inlet conditions. The increased deviation in the experiment was due to the effect of blade thickness. This fact was later confirmed by a standard Schlichting and Scholz (1951)[14] calculation which yielded an outlet angle of 47·74 degrees.

To compare theory with experiment it is necessary to derive the two dimensional flow through a cascade with camber line given by equation (17). This may be done by a standard Schlichting calculation. However, in order to simplify the computations it was assumed that the solution for Φ_{b0} could be obtained from an equivalent cascade of flat plates of zero thickness set at a stagger angle of 47·7 degrees and the same pitch-chord ratio. In other words the equation for Φ_{b0} was solved by assuming that the fourth integral term in the braces on the right hand side of equation (17) which contains the effect of thickness could be absorbed in the third term, i, by decreasing it by 2·7 degrees. In effect this was equivalent to changing the stagger or blade setting without altering the inlet flow angle. A few sample calculations showed that the error involved in this procedure was negligible.

In every calculation it was assumed that the change in axial velocity was caused by a linear contraction or divergence of the end walls inside the blade passage. The theoretical variation of mid-span outlet flow angle with AVR is also shown in Fig. 9. Although the theoretical curve was constrained to agree with the experimental result at AVR = 1, it shows very good agreement over the whole range of AVR. If the theoretical curve is approximated to a straight line, then

$$\delta = \delta_{2D} - 11{\cdot}3\,(\mathrm{AVR} - 1)$$

where δ is the deviation angle in degrees.

Fig. 10 shows the spanwise variations from tests done with solid side walls designed to contract the passage by boundary layer growth on the end walls. The measured Axial Velocity Ratio was 1·049. The agreement between theory and experiment is not very good in this case. There is no reason to expect that the wall boundary layer will cause a displacement equivalent to a linear contraction. In fact, better agreement would have been obtained if it was assumed that the wall boundary layer began to grow only in the latter half of the blade passage.

The tests done with unrestricted suction are not very suitable for comparison with the theory as measurements made one axial chord length downstream of the trailing edge plane would not have reflected the conditions far downstream. In the theory it is shown that the disturbance due to the walls (ϕ_w) causes only a uniform change in flow angle far downstream. Fig. 2 shows that the disturbance due to the walls

adjusts to its far downstream condition after about one contraction length downstream of the downstream edge of the contracting wall. If side wall suction is applied over an area larger than the blade passage, then it is necessary to make measurements farther downstream than one axial chord length from the trailing edge in order to obtain the proper downstream condition. This point should be considered in assessing the value of data from experiments with unrestricted side wall suction.

Fig. 11 shows the results from a test where side wall suction was restricted to the blade passage only. In this case the large pressure difference across the porous wall would have ensured uniform suction. Uniform wall suction would be consistent with a straight line divergence of the endwalls. The agreement between theory and experiment is good, except for slight deviations near the walls.

Fig. 12 shows the results of the test with solid contracting walls shown in Fig. 8. Of the measured Axial Velocity Ratio of 1·251, 1·2 can be accounted for by the shape of the wall. Therefore, a linear contraction of the end wall could be assumed with more confidence. There is reasonable agreement between theory and experiment; the discrepancy may be due to some boundary layer separation as described below.

As will be seen from Fig. 12 the effect of the contraction on a compressor cascade is to give a lower deflection near the walls and a higher deflection at mid-span. This effect is opposite to the effect of the endwall boundary layer shear which causes a secondary flow giving a higher deflection near the end walls. The contraction and shear effects therefore tend to counterbalance in compressor cascades. Fig. 11 shows that suction or expansion increases the deflection near the walls and therefore reinforces the shear flow effect. In a turbine cascade on the other hand the contraction effects are of opposite sign to those in compressor cascades. Expansion or 'flare' of turbine cascade end walls therfore counterbalances the effect of secondary flow or shear.

Fig. 13 shows the results of the test B2 in which a substantial shear flow at inlet was obtained by artificially thickening the boundary layer on the end walls. The results from the tests in Fig. 12 with a normal thin inlet boundary layer are shown for comparison. The AVRs in the two tests are now the same and the results are further masked by the very small or negative deflections close to the wall. Although the experimental results are disappointing the theoretical curve, when compared with those in Fig. 12, shows the counterbalancing effect mentioned above.

Fig. 14 shows the measured mid-span pressure distributions for two values of axial velocity ratio. The Martensen (1959)[9] solution for the two-dimensional pressure distribution is also shown. An outlet angle of 47·7 degrees was assumed when carrying out the Martensen calculation. The large adverse pressure gradient on the pressure surface of the aerofoil was caused by the closeness of the blade spacing. The growth of the boundary layer was calculated using the approximate method due to Thwaites (1949)[16] and it was found the laminar separation occurred at a distance 0·6 chord from the leading edge according to criteria given by Dunham (1972)[1]. It is possible that laminar separation occurs on the pressure surface in every experimental pressure distribution shown. Separation can reduce the diffusing action of the latter part of the blade passage and yield trailing edge inviscid pressures lower than those calculated by potential flow methods. The result that the trailing edge pressure for AVR = 0·943 is less rather than greater than the two-dimensional potential flow value may be due to this separation. Fig. 15 shows the variation of pressure distribution along the span in the test with solid contracting end walls. It should be noted that, due to blade thickness and the closeness of the spacing, all pressure distributions show negative lift near the leading edge.

It was possible to calculate the variation of pressure distribution along the span by solving the $n = 0$ term by a Schlichting type method which takes into account blade thickness and then adding the other, three-dimensional terms later (Galappatti (1973)[2]). The results of one such calculation are presented in Fig. 16 and the theoretical curves appear to predict the trends observed in the experiments (Fig. 15).

6. Conclusion

The small perturbation theory which has been developed for endwall contraction or expansion of the flow through linear cascades of compressor or turbine blades shows that earlier methods, which depended on a spanwise integration of the flow equations, are in error, because they do not allow for the variation of circulation along the blades and the effect of the induced velocities produced by the consequent shed vorticity. The work shows that Axial Velocity Ratio is not the only significant parameter governing the effects of endwall contraction and that the aspect ratio, the stagger angle, and the pitch-chord ratio as well as the shape and position of the contraction or expansion, and endwall suction, also have an influence. The experimental results from a cascade of symmetrical uncambered aerofoils spaced at such a small pitch chord ratio and tested at such a low angle of attack that only a few degrees of deflection were obtained were affected by the large diffusion on the pressure surfaces which probably caused some separation. Nevertheless

most of the eight experiments confirmed the theoretical predictions satisfactorily and those with porous endwall suction demonstrated the need for considerable care in cascade experiments with porous walls to ensure that the suction through the walls is restricted to an area which does not affect the measurements made downstream of the cascade.

An extension of the theory to allow for the shear flow at the end walls produced by substantial inlet boundary layers as well as contraction or expansion indicates that secondary flows induced by this shear may be reduced by endwall contraction in compressor cascades or by expansion in turbine cascades.

An important conclusion is that the use of empirical correlations of the effects of Axial Velocity Ratio should be used with greater care in the calculations of flow through compressors and turbines.

LIST OF SYMBOLS

A_k	Given by equation (71)
A_n	Given by equation (7)
AVR	Axial Velocity Ratio
$a(x_1)$	Wall shape
C_L	Lift coefficient
C_p	Pressure rise coefficient
c	Chord length
$F(k)$	Coefficient in equation (74)
$f(x_1)$	Source strength on wall
$G(k)$	Coefficient in equation (67)
h	Width of passage in spanwise direction
i	Angle between inlet flow and blade chord
K_0	Modified Bessel function of the second kind of order zero.
k	Eigen value
k_n	Constant in equation (43)
l	Aspect ratio
M	Doublet strength
M'	Non-singular solution
m	Summation index
N	Singular solution
n	Number of Fourier terms
p	Pressure
q	Strength of sources along chord line
R_m	Given by equation (28)
S	Given by equation (16)
s	Pitch chord ratio
T	Half the thickness of blade
U	Mainstream velocity
u, v, w	Components of disturbance velocity
$\bar{u}, \bar{v}, \bar{w}$	Pitchwise averaged velocities
x, y, z	Co-ordinate axes based on inlet flow direction
x_1, y_1, z_1	Co-ordinate axes based on cascade line
Z	Eigenfunction
β	Flow deflection
γ	Circulation on aerofoil
δ	Deviation angle
$\delta(x)$	Dirac's delta function
$\zeta(x)$	Equation of camber line with respect to chord line
θ	Camber angle
λ	Inlet flow angle
ξ	Co-ordinate of singularity distribution along x-axis
ρ	Density of fluid
Φ	Potential function
ϕ	Velocity potential or potential function

$$\nabla \qquad \mathbf{i}\frac{\partial}{\partial x}+\mathbf{j}\frac{\partial}{\partial y}+\mathbf{k}\frac{\partial}{\partial z}$$

$$\nabla^2 \qquad \frac{\partial^2}{\partial x^2}+\frac{\partial^2}{\partial y^2}+\frac{\partial^2}{\partial z^2}$$

$$\nabla_2^2 \qquad \frac{\partial^2}{\partial x^2}+\frac{\partial^2}{\partial y^2}=\frac{\partial^2}{\partial x_1^2}+\frac{\partial^2}{\partial y_1^2}$$

Subscripts

b	Disturbance due to thin blades
$2D$	Two-dimensional flow without endwall contraction
n	Number of Fourier terms
t	Disturbance due to blade thickness
t.e.	Trailing edge
w	Disturbance due to the walls

REFERENCES

No.	Author(s)	Title
1	J. Dunham	Predictions of boundary layer transition on turbomachinery blades. Agardograph No. 164, pp. 55–75 (1972).
2	R. Galappatti	Cascades with end wall contraction. Ph.D. Thesis, Cambridge University (1973).
3	M. Honda	Theory of shear flow through a cascade. Proc. Roy. Soc. A, 265, pp. 46–70 (1961).
4	J. H. Horlock	*Axial flow compressors.* Butterworths, London, pp. 105–114 (1958).
5	D. R. Kotansky	Thin airfoils in rotational flow. M.I.T. Gas Turbine laboratory report No. 80 (1965).
6	B. Lakshminarayana	NASA SP-304 pp. 127 (1974) (*see* Ref. 8).
7	R. Mani and A. J. Acosta	Quasi-two-dimensional flows through a cascade. Trans. A.S.M.E., *J. Engng. for Power*, 90, 2, pp. 119–128 (1968).
8	R. Mani, A. J. Acosta and M. B. Wilson	A note on the influence of axial velocity ratio on cascade performance. NASA SP-304, pp. 101–122 (1974).
9	E. Martensen	Calculation of the pressure distributions over profiles in cascade in two-dimensional potential flow by means of a Fredholm integral equation. *Archive for Rational Mathematics and Analysis*, Vol. 3, 3 (1959).
10	M. C. Nally and W. R. Hawthorne	A numerical solution for shear flow through a cascade of aerofoils. N.E.L. report 432 (1969).
11	M. Namba	Lifting surface theory for a cascade of aerofoils in subsonic shear flow. *J. Fluid Mech.*, Vol. 36, pp. 735–757 (1969).
12	D. Pollard and J. H. Horlock	A theoretical investigation of the effect of change in axial velocity on the potential flow through a cascade of aerofoils. A.R.C. C.P. No. 619 (1962).
13	J. W. Railly	The design of mixed flow cascades by Ackeret's Method. *The Engineer*, Vol. 224, 5827, pp. 405–416 (1967).
14	H. Schlichting and N. Scholz	Ueber die theoretische berechnung der stroemungsverluste eines ebenen schaufelgitters. *Ing. Arch.*, Vol. 19, pp. 42–65 (1951).
15	M. R. A. Shaalan and J. H. Horlock	The effect of change in axial velocity on the potential flow in cascades. A.R.C. R. & M. No. 3547 (1968).

No.	*Author*	*Title*
16	B. Thwaites	Approximate calculation of the laminar boundary layer. *Aero. Quart.*, Vol. 1, pp. 245–280 (1949).

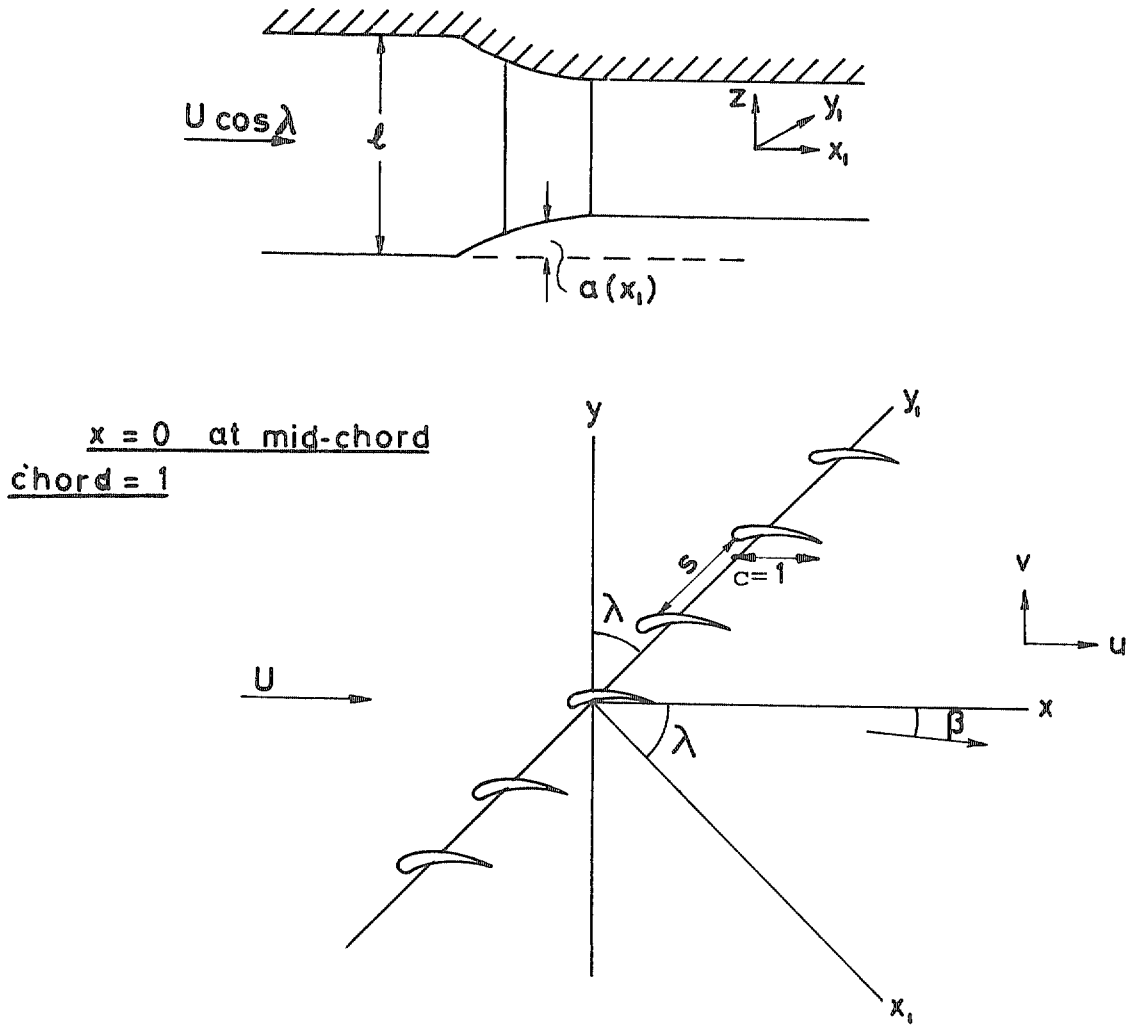

FIG. 1. Cascade with contracting end walls.

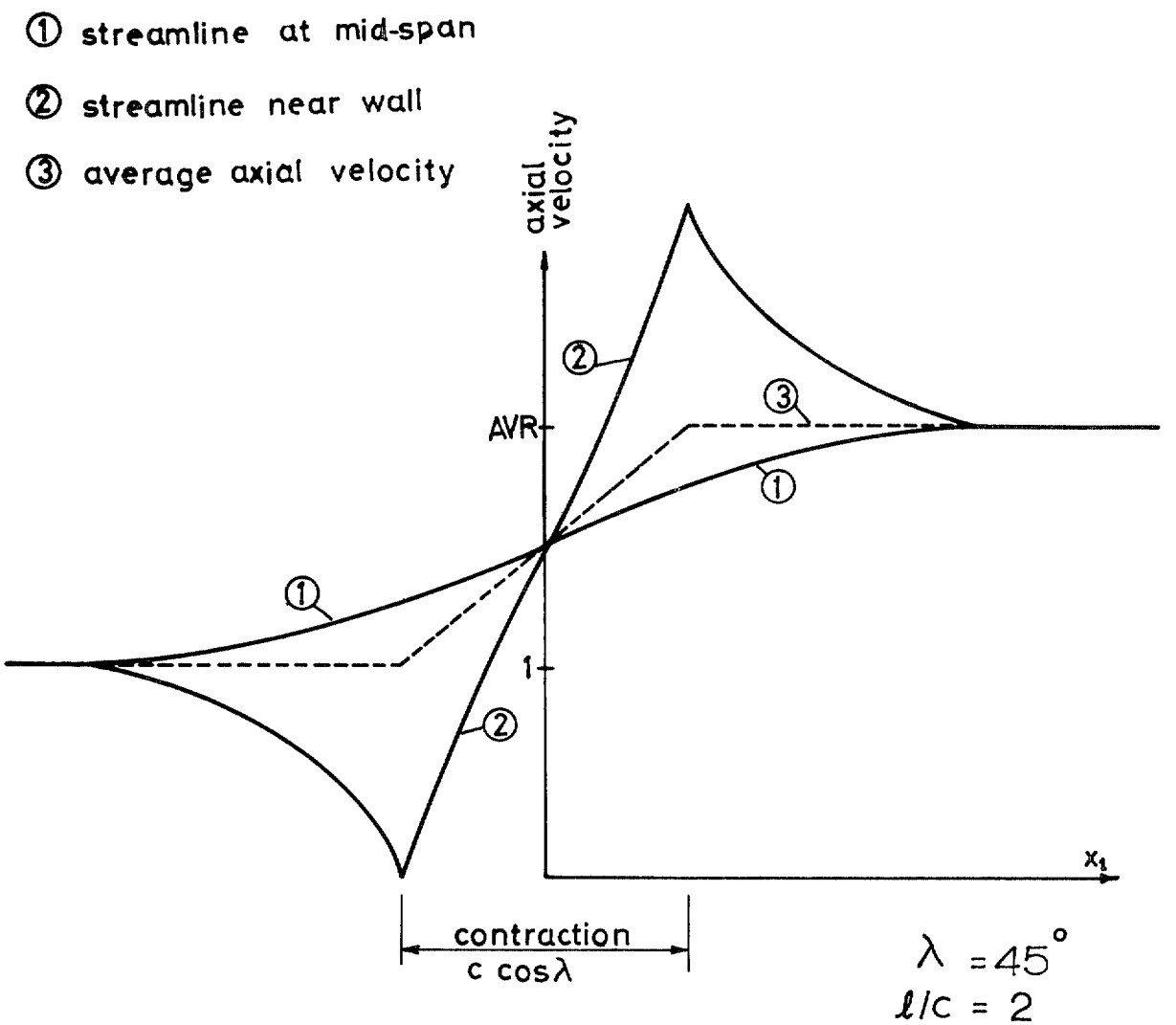

FIG. 2. Variation of axial velocity in duct with linear end wall contraction.
(1) Mid span streamline
(2) Streamline near wall;
(3) Average across span.

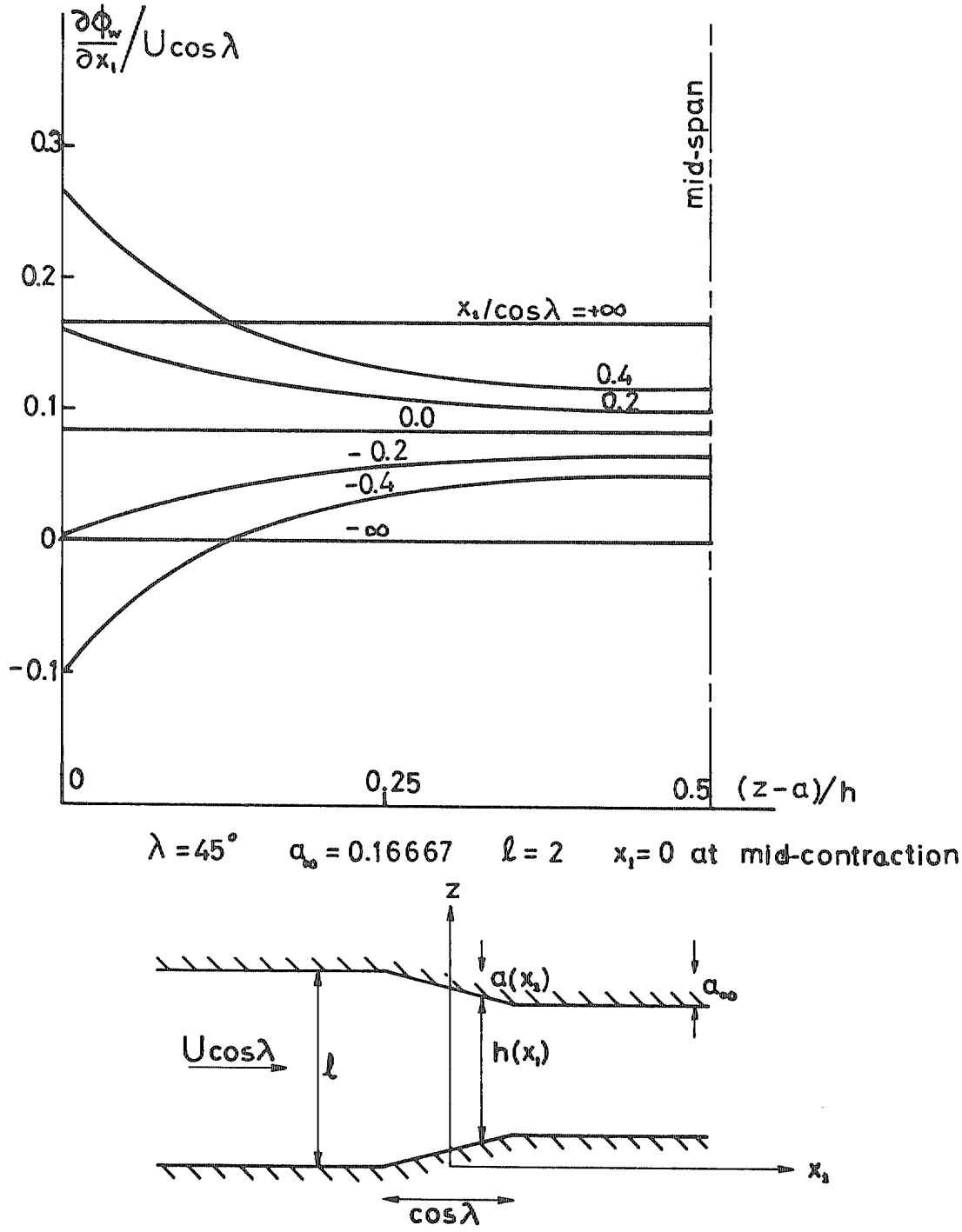

FIG. 3. Variation of axial velocity across duct with linear end wall contraction at different axial stations.

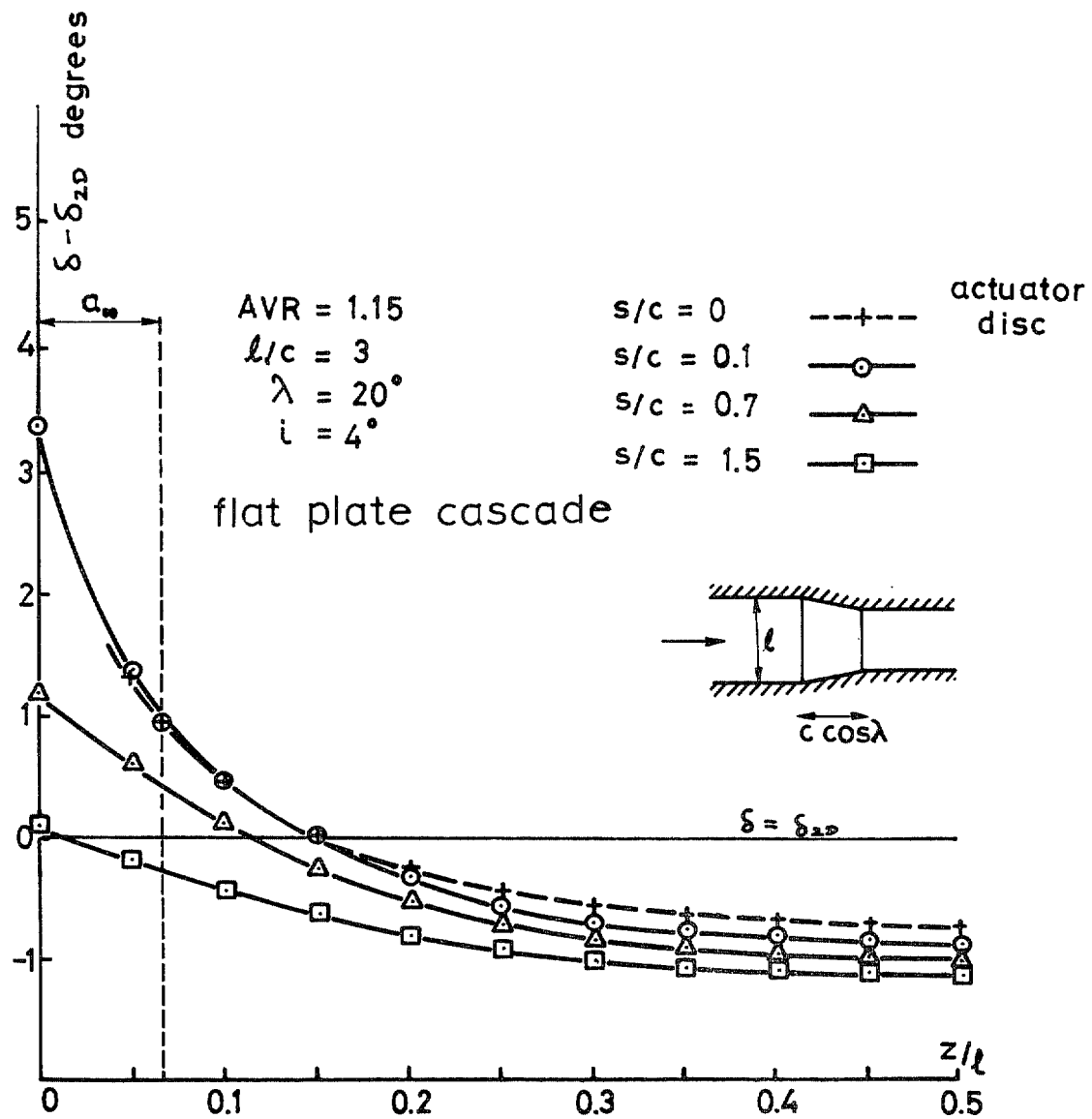

FIG. 4. Spanwise variation of deviation.

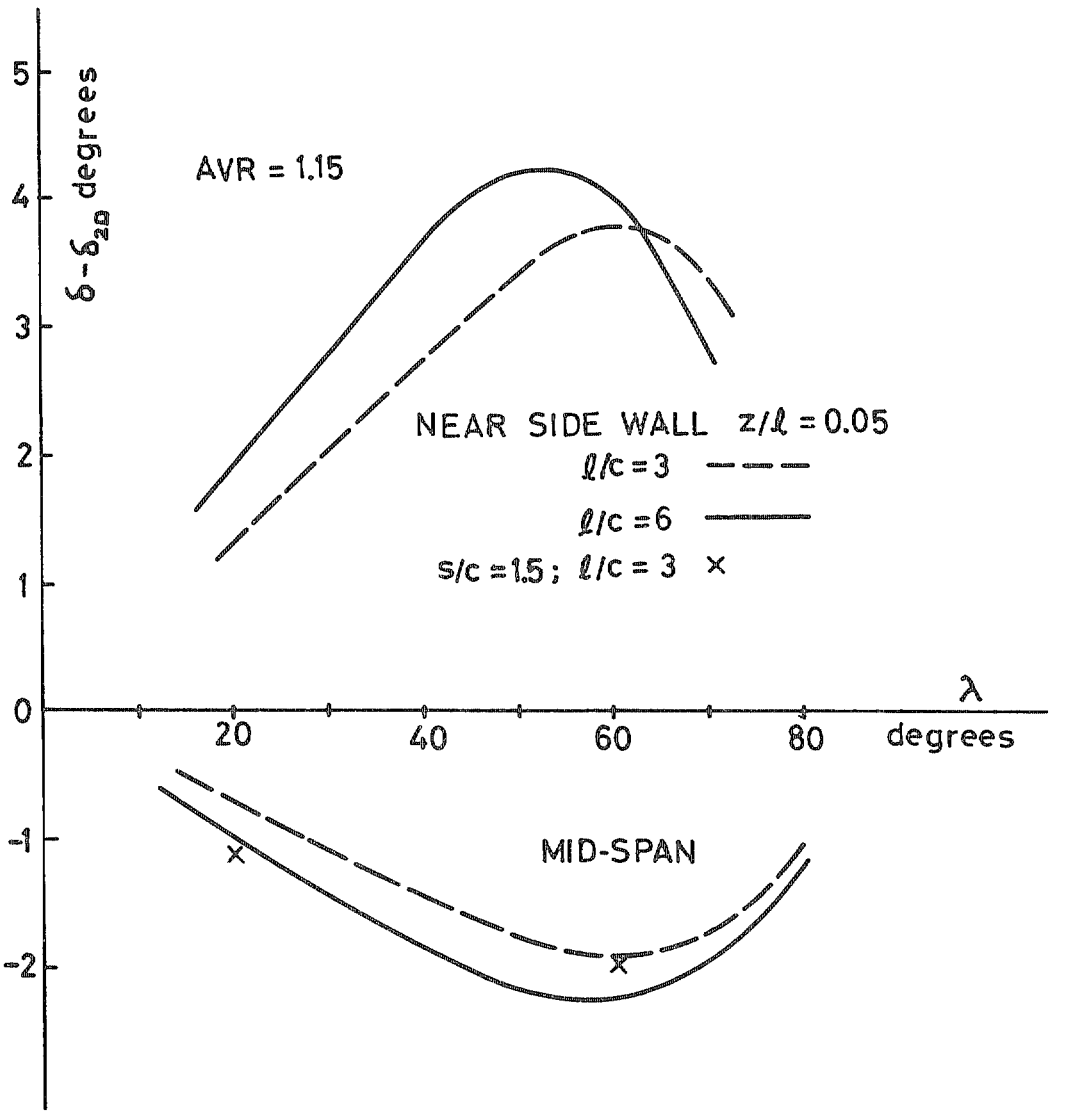

FIG. 5. Variation of deviation with inlet flow angle (actuator disc solution).

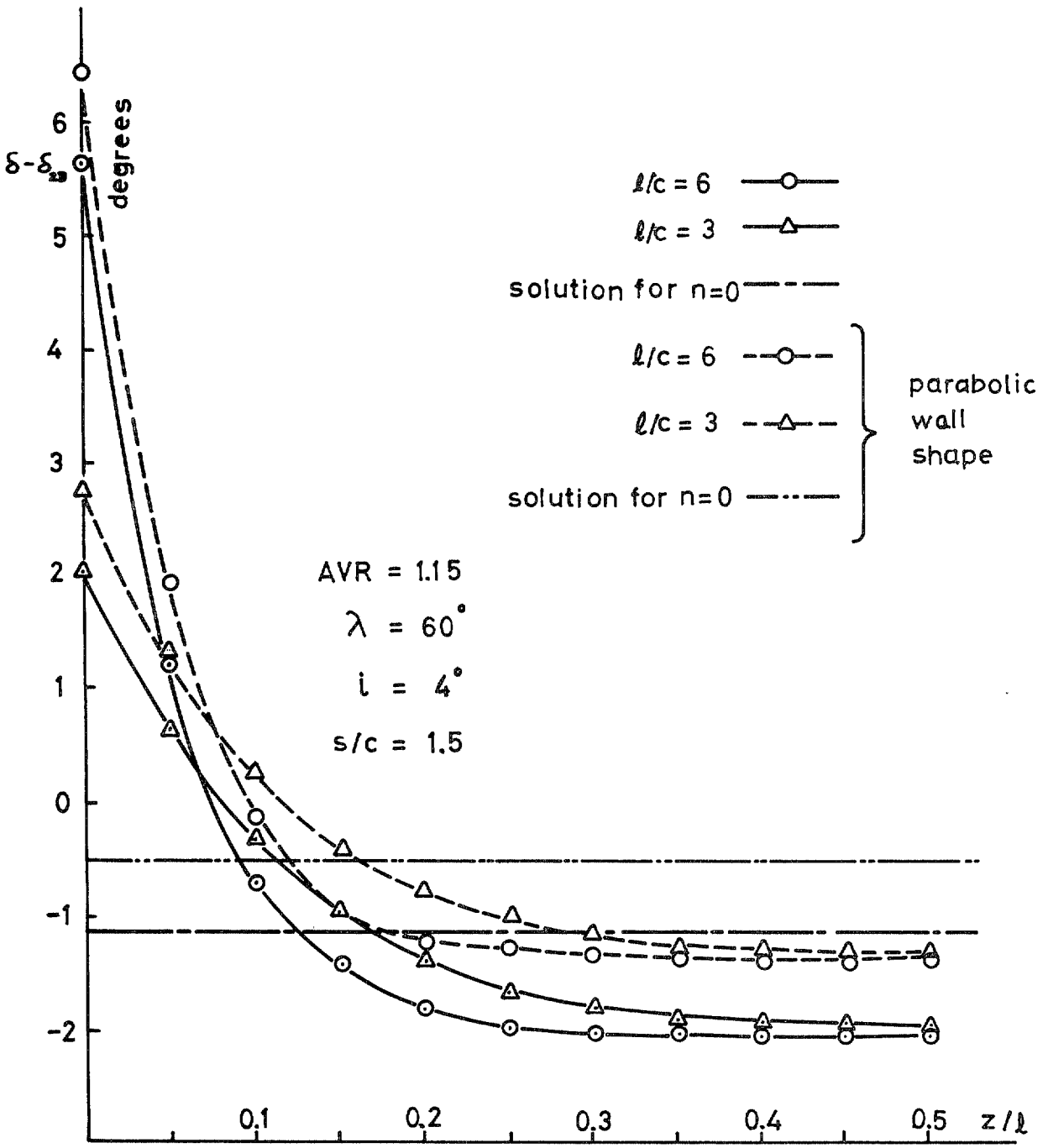

FIG. 6. Spanwise variation of deviation (theory—flat plate cascade).

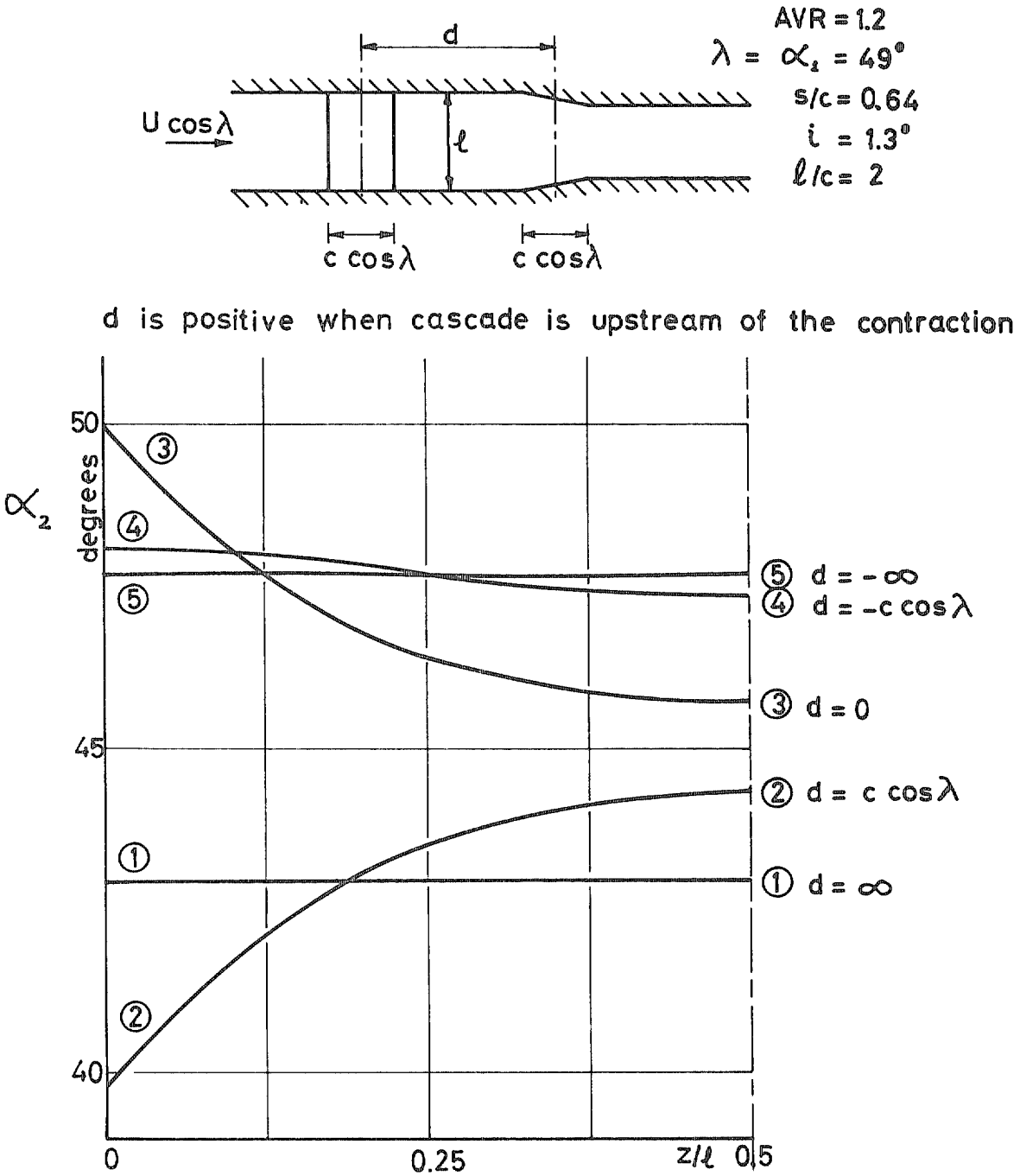

FIG. 7. The influence of the position of the contraction on the flow angle far downstream.

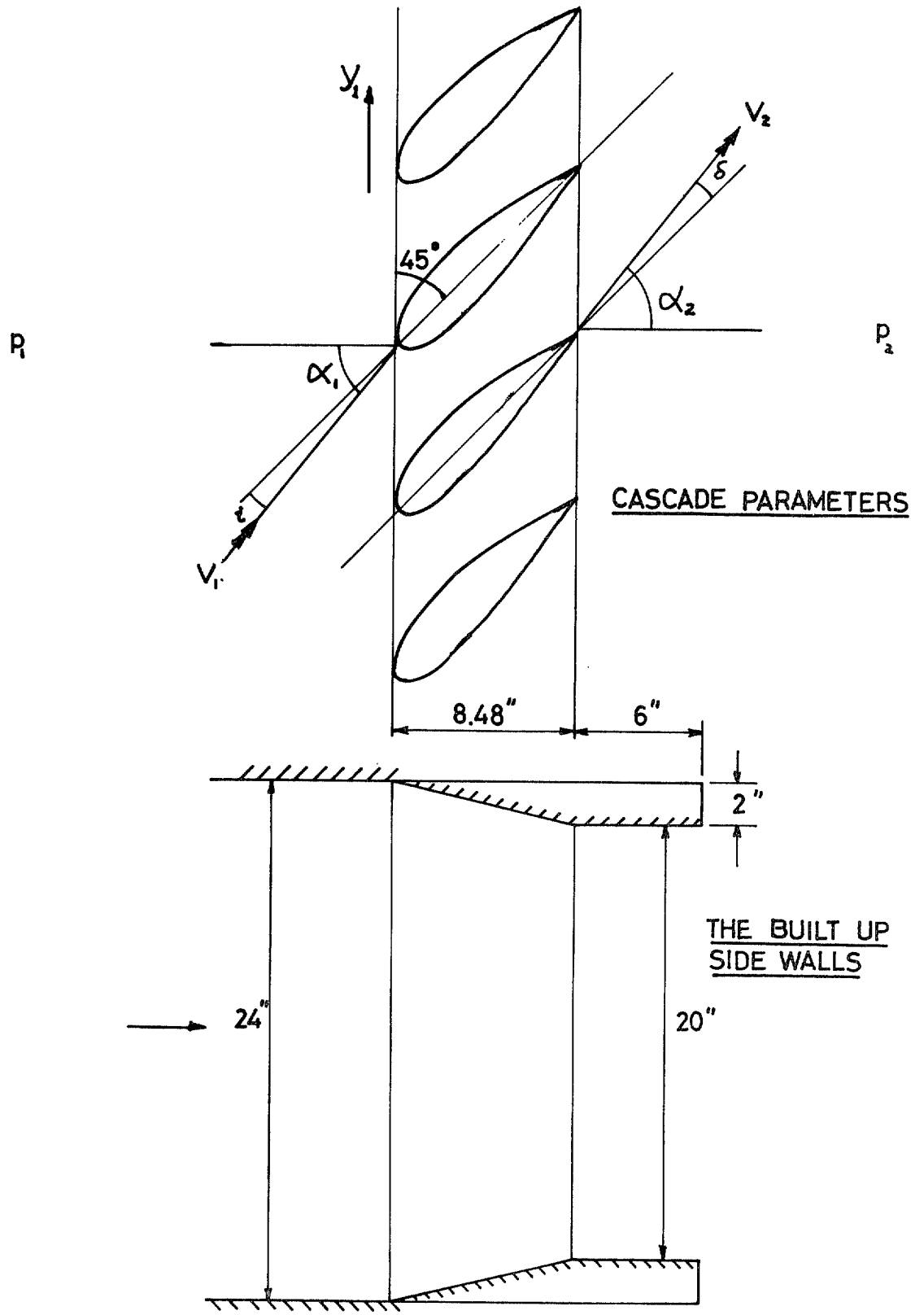

FIG. 8. Cascade geometry and nomenclature.

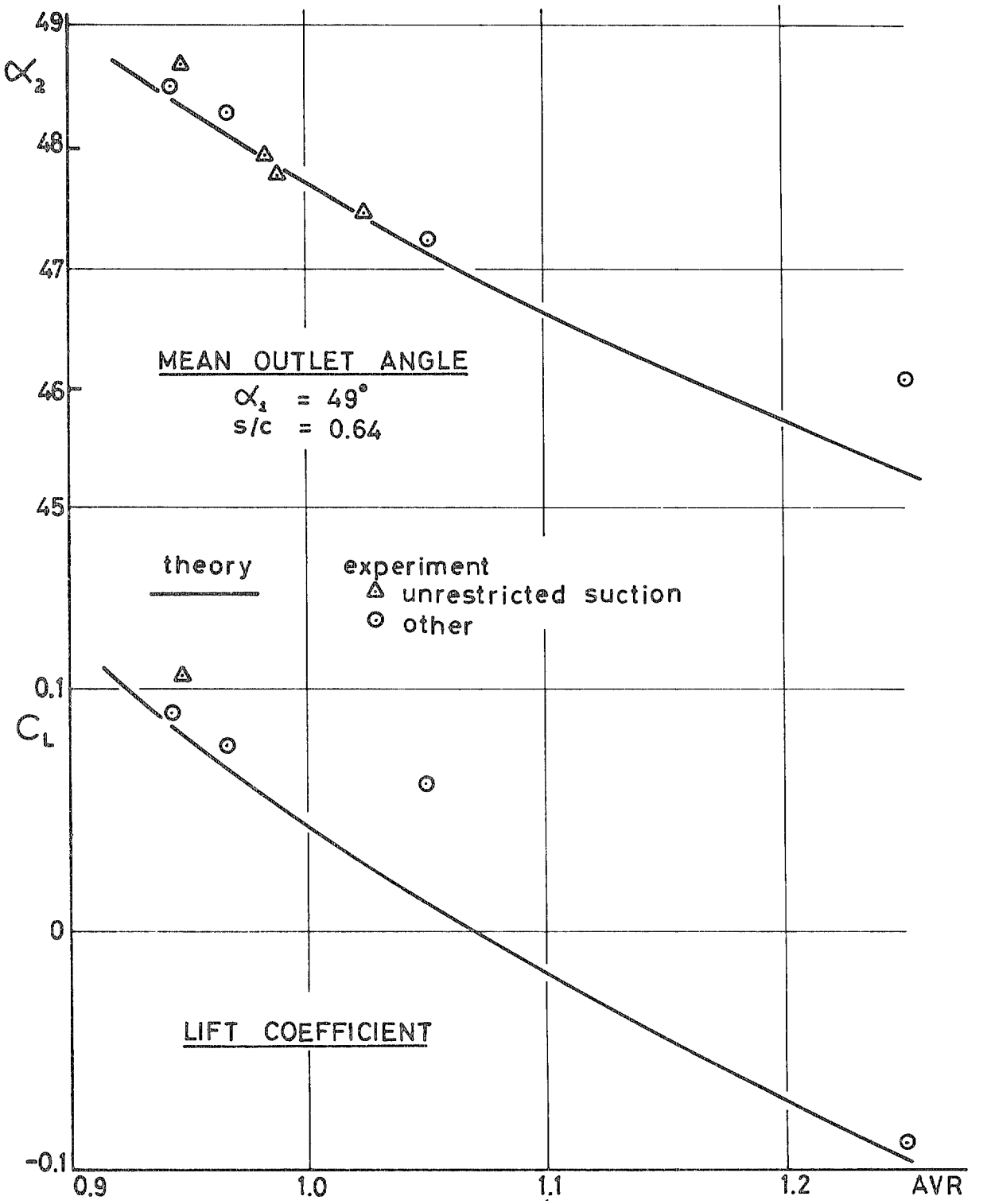

FIG. 9. Variation of outlet angle and lift at mid span with AVR.

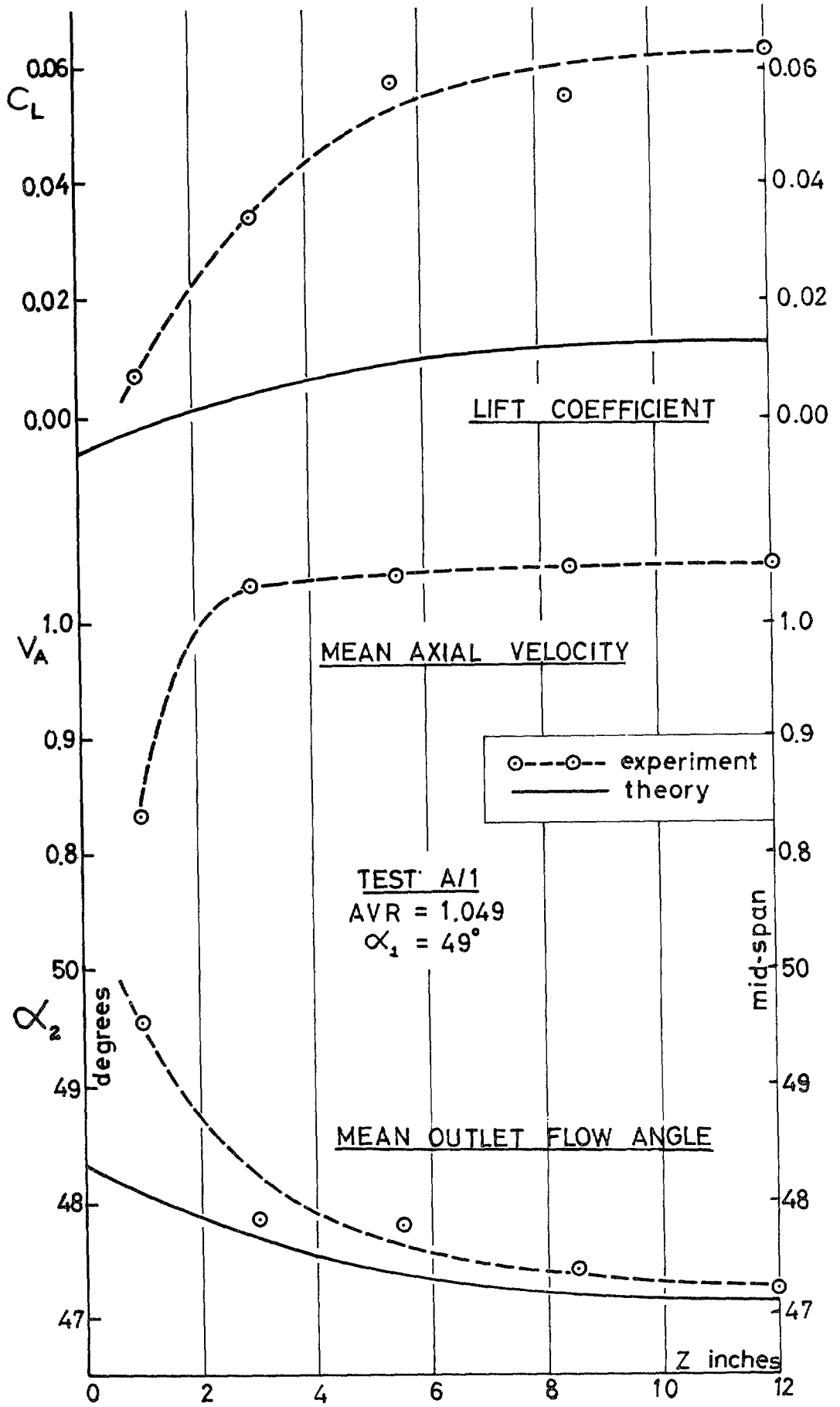

FIG. 10. Results of solid wall test (A/1).

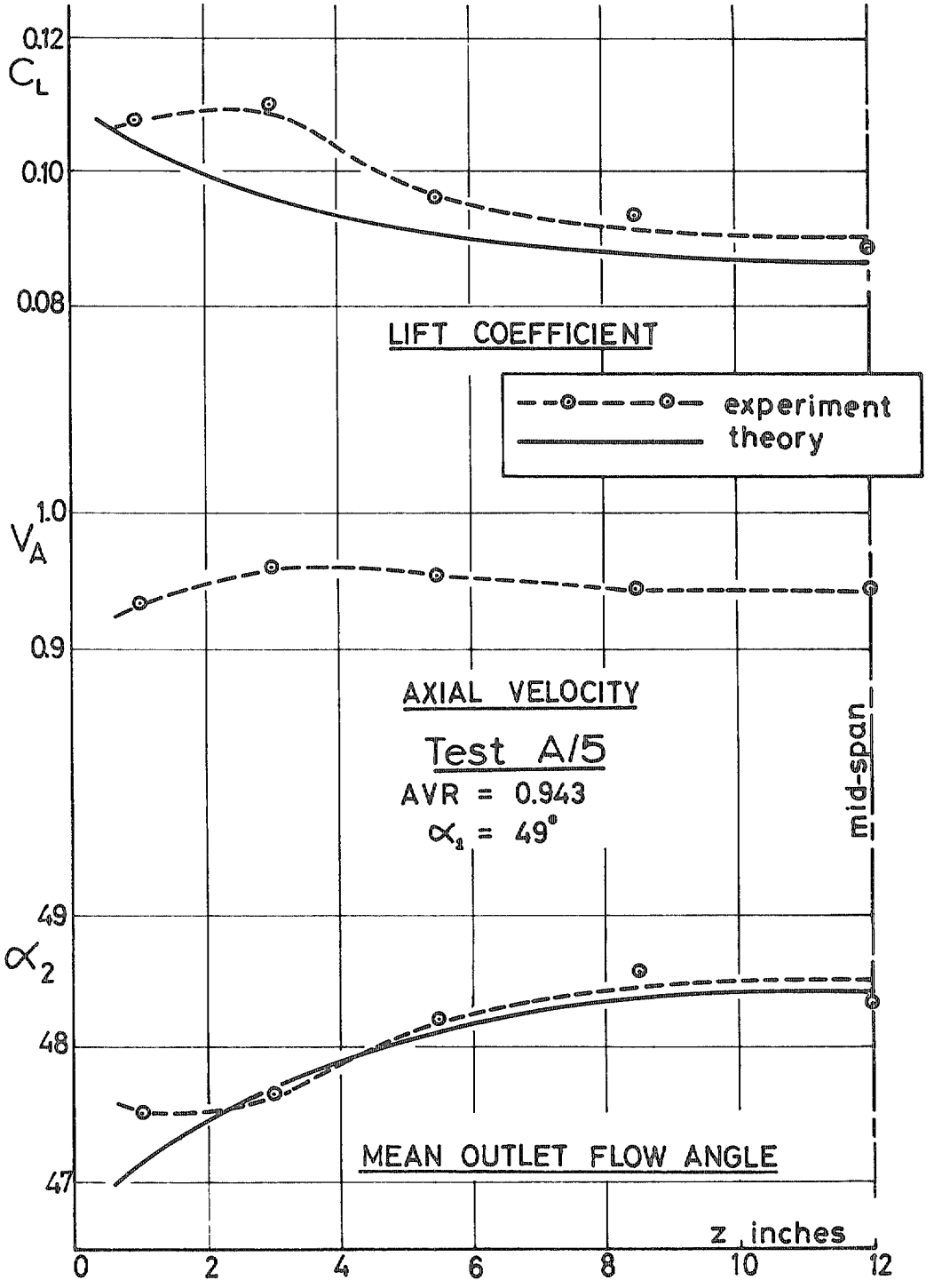

FIG. 11. Results of test with restricted suction (A/5).

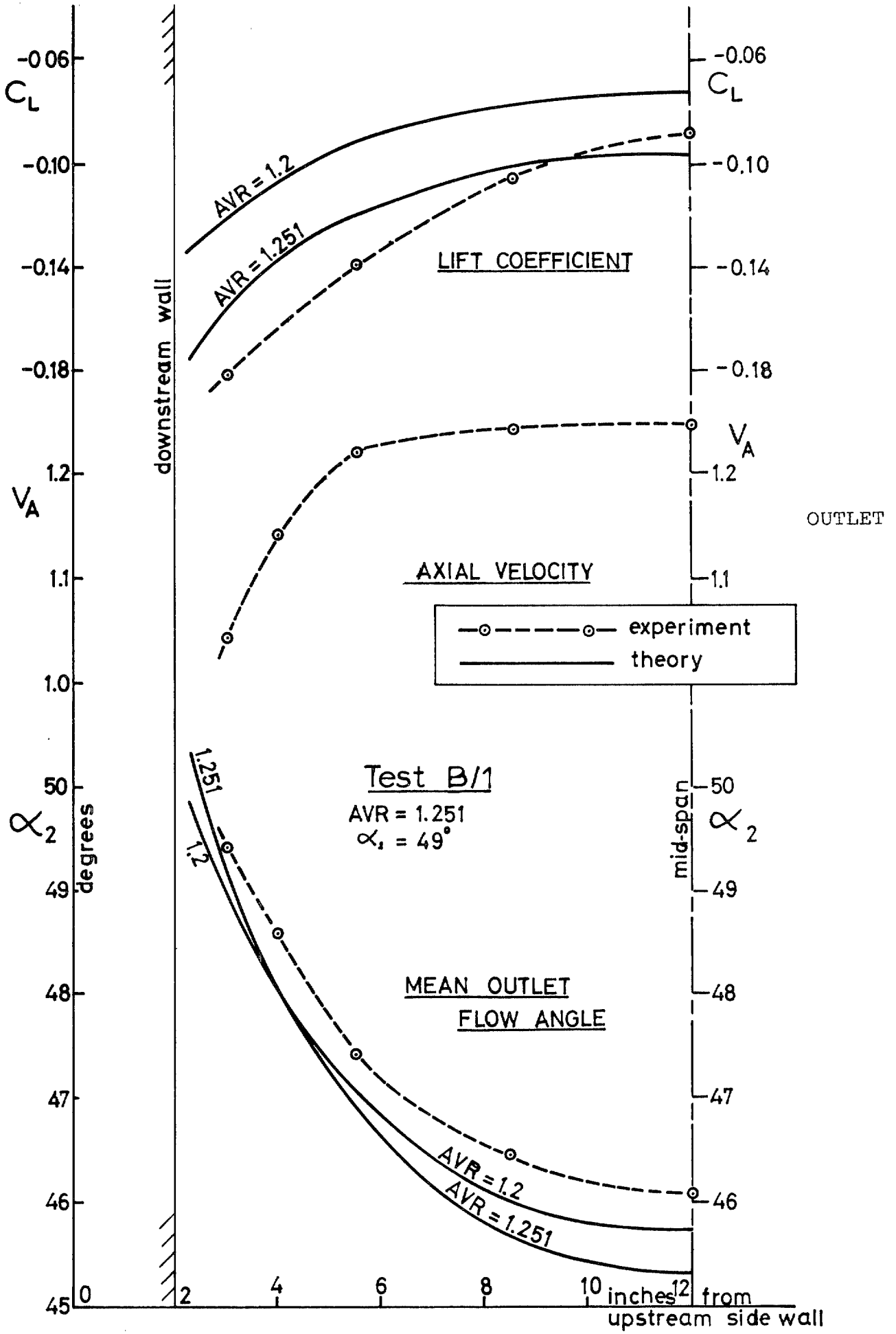

FIG. 12. Results of test with contracting end walls (B/1).

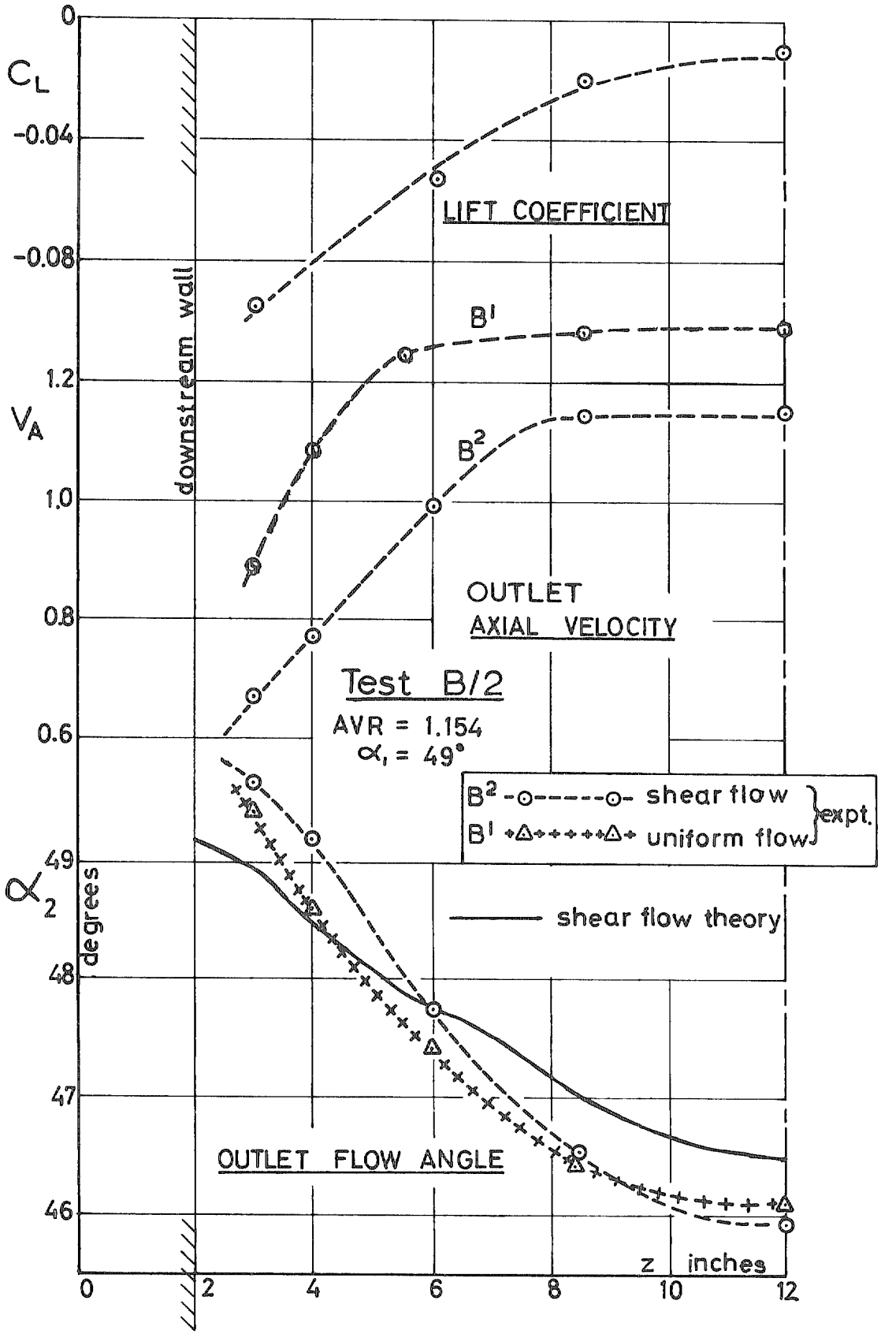

FIG. 13. Results of tests with shear and contraction (B2), compared with B1.

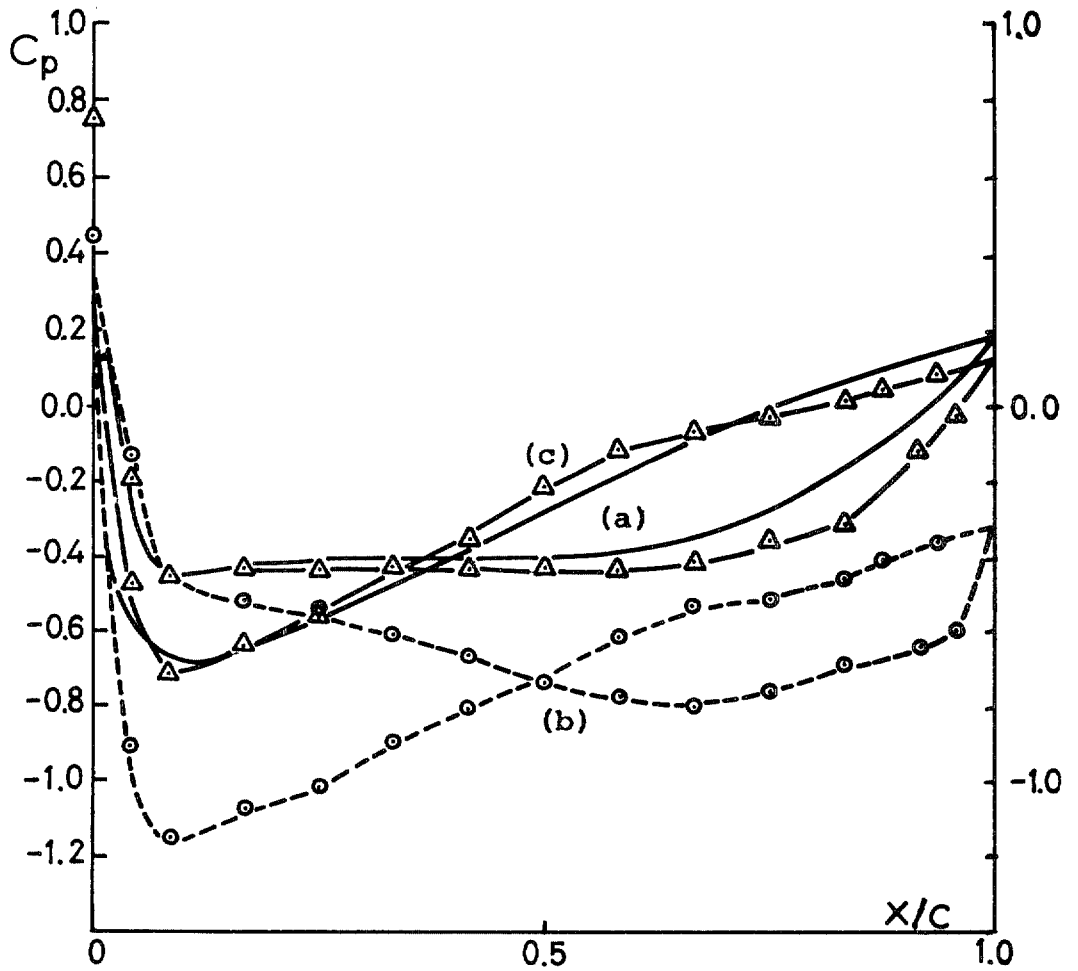

FIG. 14. Pressure distributions at midspan.
(a) Martensen calculation AVR = 1·0
(b) Test B1 AVR = 1·25
(c) Test A5 AVR = 0·943

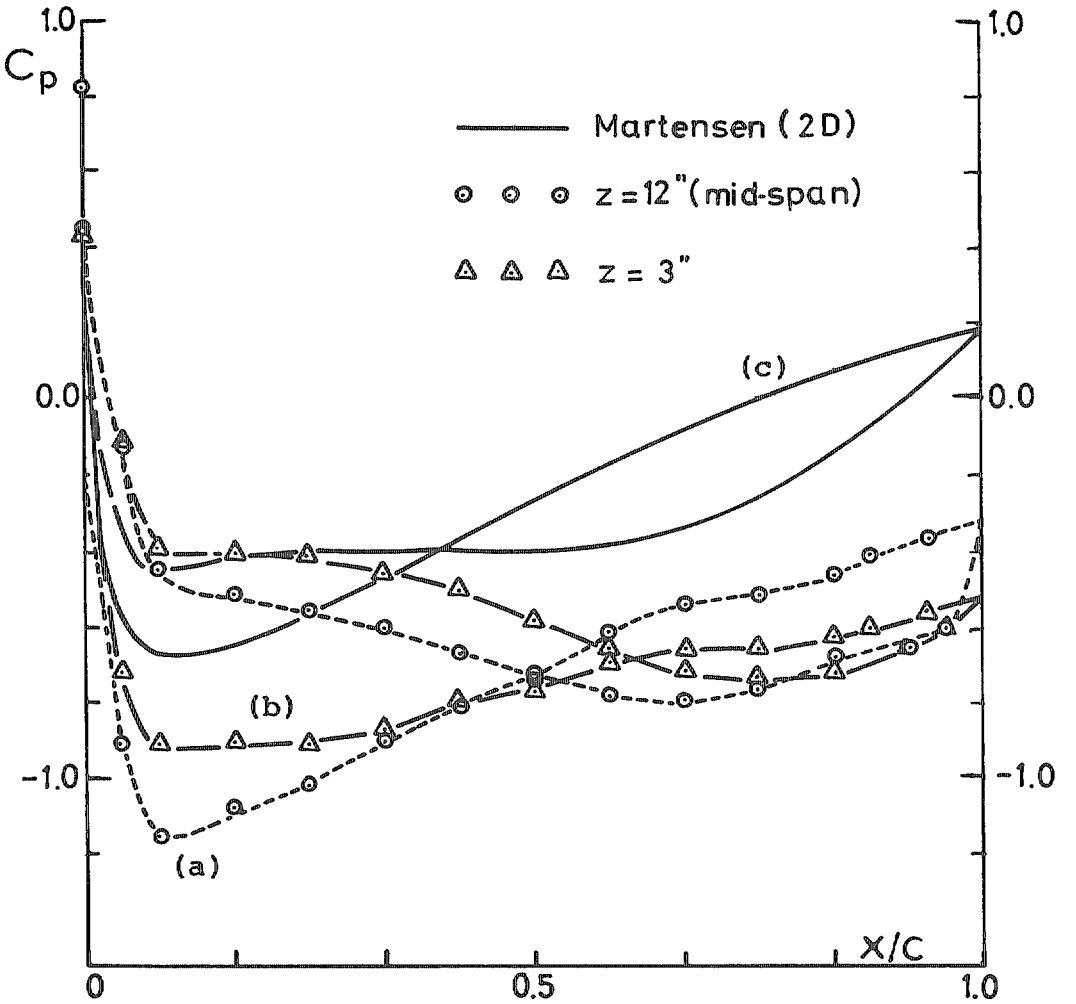

FIG. 15. Measured pressure distributions for test with contracting end walls. (B/1) AVR = 1·251.
(a) Mid-span $z = 12$ in.
(b) $z = 3$ in. (note downstream wall at $z = 2$ in.)
(c) Martensen two-dimensional theoretical solution.

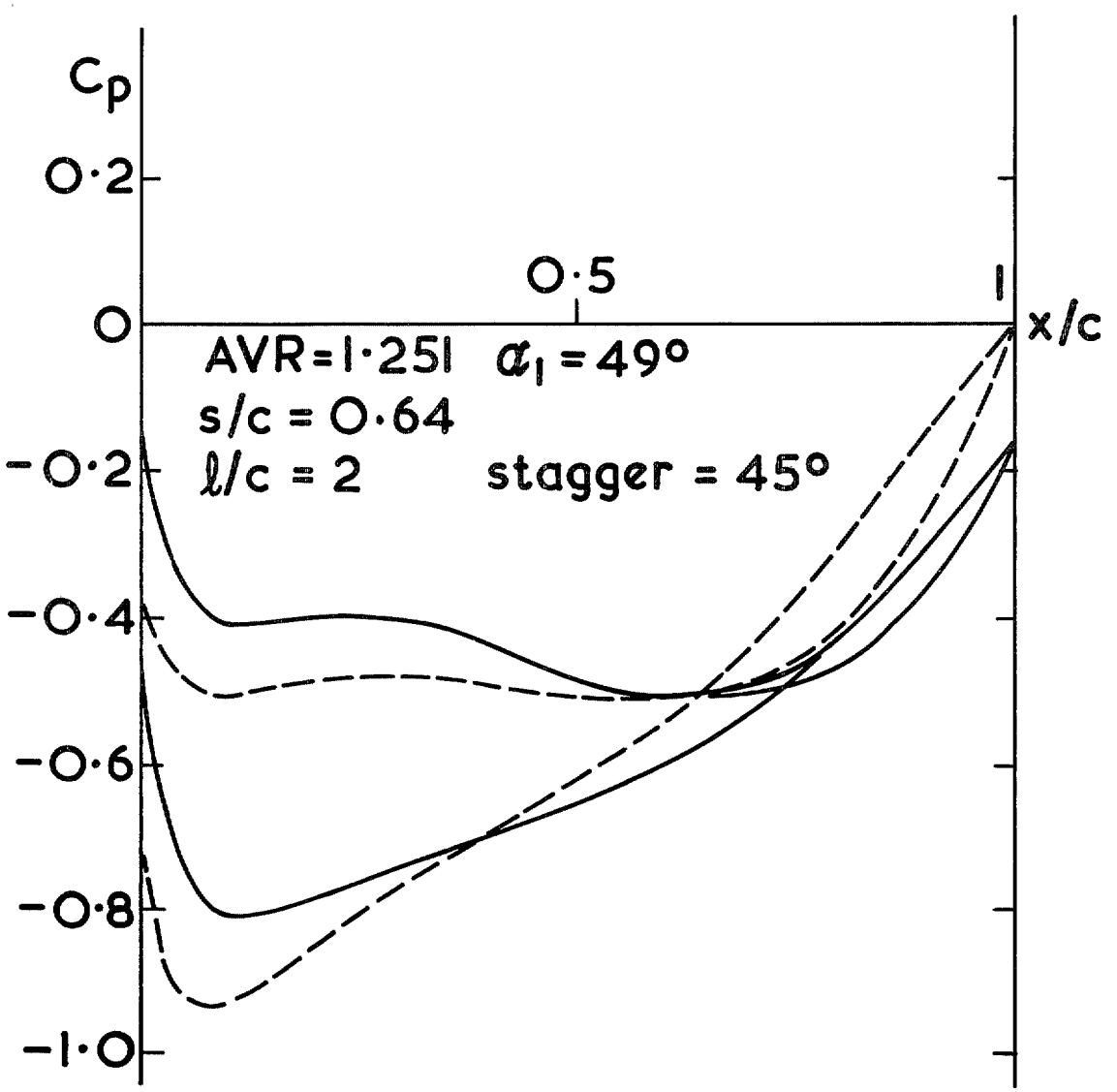

FIG. 16. Theoretical pressure distributions.

AVR = 1·251, $s/c = 0{\cdot}64$, $l/c = 2$, stagger = 45°, $\alpha_1 = \lambda = 49°$.

——— mid span, $C_L = -0{\cdot}115$.

——— $z = 0{\cdot}05l$. $C_L = -0{\cdot}158$.

Printed in England for Her Majesty's Stationery Office by J. W. Arrowsmith Ltd., Bristol BS3 2NT
Dd. 587484 K.5. 2/78.

HER MAJESTY'S STATIONERY OFFICE

Government Bookshops

49 High Holborn, London WC1V 6HB
13a Castle Street, Edinburgh EH2 3AR
41 The Hayes, Cardiff CF1 1JW
Brazennose Street, Manchester M60 8AS
Southey House, Wine Street, Bristol BS1 2BQ
258 Broad Street, Birmingham B1 2HE
80 Chichester Street, Belfast BT1 4JY

Government Publications are also available through booksellers

R. & M. No. 3813

ISBN 0 11 471146 1